Journal of Solid State Chemistry 181 (2008) 2205–2216

Contents lists available at ScienceDirect

Journal of Solid State Chemistry

journal homepage: www.elsevier.com/locate/jssc

0-D and 1-D inorganic–organic composite polyoxotungstates constructed from in-situ generated monocopper^{II}-substituted Keggin polyoxoanions and copper^{II}–organoamine complexes

Jun-Wei Zhao, Shou-Tian Zheng, Guo-Yu Yang *

State Key Laboratory of Structural Chemistry, Fujian Institute of Research on the Structure of Matter and Graduate School of the Chinese Academy of Sciences, Fuzhou, Fujian 350002, PR China

ARTICLE INFO

Article history:
Received 16 January 2008
Received in revised form
17 April 2008
Accepted 27 April 2008
Available online 14 May 2008

Keywords:
Polyoxometalate
Hydrothermal reaction
Copper
Keggin structure
Organoamine

ABSTRACT

Combination of in-situ generated monocopper^{II}-substituted Keggin polyoxoanions with copper^{II}–organoamine complexes under hydrothermal conditions results in seven inorganic–organic composite polyoxotungstates $[Cu(en)_2(H_2O)]_2\{[Cu(en)_2][\alpha\text{-}PCuW_{11}O_{39}Cl]\}\cdot 3H_2O$ (**1**), $\{[Cu(en)_2(H_2O)][Cu(en)_2]_2[\alpha\text{-}PCuW_{11}O_{39}Cl]\}\cdot 6H_2O$ (**2**), $\{[Cu(en)_2(H_2O)]_2[Cu(en)_2][\alpha\text{-}XCuW_{11}O_{39}]\}\cdot 5H_2O$ (**3**/**4**, $X = Si^{IV}/Ge^{IV}$), $\{[Cu(deta)(H_2O)_2]_2[Cu(deta)(H_2O)][\alpha\text{-}XCuW_{11}O_{39}]\}\cdot 5H_2O$ (**5**/**6**, $X = Ge^{IV}/Si^{IV}$) and $[Cu(dap)_2]_2\{[Cu(dap)_2]_2[Cu(dap)_2][\alpha\text{-}PCuW_{11}O_{39}]_2\}$ (**7**) (en = ethylenediamine, dap = 1,2-diaminopropane and deta = diethylenetriamine). **1** is an isolated structure whereas **2** is a 1-D chain structure, but both contain $[\alpha\text{-}PCuW_{11}O_{39}Cl]^{6-}$ polyoxoanions. **3–6** contain the 1-D linear chains made up of $[\alpha\text{-}XCuW_{11}O_{39}]^{6-}$ polyoxoanions in the pattern of –*A*–*A*–*A*– ($A = [\alpha\text{-}XCuW_{11}O_{39}]^{6-}$), while **7** demonstrates the first 1-D zigzag chain constructed from $[\alpha\text{-}PCuW_{11}O_{39}]_2^{10-}$ polyoxoanions via $[Cu(en)_2]^{2+}$ bridges in the pattern of –*A*–*B*–*A*–*B*– ($A = [\alpha\text{-}PCuW_{11}O_{39}]_2^{10-}$, $B = [Cu(en)_2]^{2+}$). The successful syntheses of **1**–**7** can provide some experimental evidences that di-/tri-/hexa-vacant polyoxoanions can be transformed into mono-vacant Keggin polyoxoanions under hydrothermal conditions.

1. Introduction

Polyoxometalates (POMs) have been known for almost two centuries [1], until 1934, the first structural detail was determined by Keggin [2]. From then on, the worldwide interest in POMs and the rate of discovering novel species have steadily increased. Historically, the successful industrialization of the production of isopropylalcohol by hydration of propylene catalyzed by $H_4SiW_{12}O_{40}$ in Japan in 1972 further inspires the extensively increasing interest throughout the world [3]. Hitherto, POMs have developed to a rapidly growing family of inorganic oxide clusters bearing more commercial applications than other cluster compounds [4,5]. The significantly current attraction in POM chemistry have been provoked not only by their surprising compositional and structural variability, but also by their versatile applications in catalysis, medicine, material science, magnetism and photochemistry, etc. [6–12].

It has been long recognized that the incorporation of transition-metal complexes (TMCs) to the inorganic POM surfaces or framework provides a quite powerful method for the design and synthesis of novel inorganic–organic composite materials that bear both features of inorganic and organic components. The TMCs introduced can work as either charge compensation cations, modify inorganic POM surfaces and frameworks, or connect discrete clusters into multi-dimensional ordered arrays [5]. To date, the search for inorganic–organic composite Keggin-based materials continues to dominate the forefront of POM chemistry. Although many plenary Keggin-based TMCs or rare-earth complexes have been reported [13–17], the systematic investigation on inorganic–organic composite mono-vacant Keggin-based POM derivatives is less developed [18–25]. For instance, $[ET]_8[PMnW_{11}O_{39}]\cdot 2H_2O$ [18], (ET = bis(ethylenedithio)tetrathiofulvalene) and $[NEt_3H]_5[XCoW_{11}O_{39}]\cdot 3H_2O$ ($X = P^V$ or As^V) [19] contain a 1-D chain structure, in which organic components only act as charge compensation cations. Additionally, $[Co(dpa)_2(OH_2)_2]_2[Hdpa][PCoW_{11}O_{39}]$ (dpa = di-2-pyridylamine) [20], $[Cu(en)_2(H_2O)][\{Cu(en)_2\}_2SiCuW_{11}O_{39}]\cdot 7H_2O$ [21], and $[H_2bpy][Cu(4,4'\text{-}bpy)]_2[HPCuMo_{11}O_{39}]$ [22] were all synthesized using sodium tungstate rather than POM precursors under hydrothermal conditions. Recently, Gutiérrez-Zorrilla et al. synthesized and characterized a series of hybrids constructed from monocopper^{II}-substituted Keggin polyoxoanions and copper^{II} complexes by means of mono-vacant Keggin precursors in the acetic acid/alkaline acetate buffer solution and also investigated the influence of alkaline cations of

* Corresponding author. Fax: +86 591 8371 0051.
E-mail addresses: guoyu.yang@hotmail.com, ygy@fjirsm.ac.cn (G.-Y. Yang).

0022-4596/$ - see front matter © 2008 Elsevier Inc. All rights reserved.
doi:10.1016/j.jssc.2008.04.042

buffer compositions on the dimensionality of the resulting products [23–25]. In addition, the mono-vacant Keggin-based rare-earth derivatives with 1-D polymeric chains have been extensively surveyed by conventional aqueous solution methods [26–31].

Currently, our interest is focused on exploiting the system containing di-/tri-/hexa-vacant POM precursors, copper^{II} salts and organoamines under hydrothermal conditions with regard to the following considerations: (a) available surface oxygen atoms on polyoxoanions possess the high nucleophilicity and reaction activity; (b) the lacunary sites on polyoxoanions can work as structure-directing agents and induce the formation and aggregation of novel POM clusters; (c) introduction of Cu^{II} cations allows multi-dimensional structures via long Cu–O distances due to the Jahn–Teller distortion. In our search, two novel hexa-Cu^{II}-substituted polyoxotungstates (POTs) $[Cu(enMe)_2]_2\{[Cu(enMe)_2(H_2O)]_2[Cu_6(enMe)_2(B\text{-}\alpha\text{-}SiW_9O_{34})_2]\}\cdot 4H_2O$ [32] and $[Cu_6(\mu_3\text{-}OH)_3(en)_3(H_2O)_3(B\text{-}\alpha\text{-}PW_9O_{34})]\cdot 7H_2O$ [33] have been isolated. Furthermore, three unprecedented octa-Cu^{II} sandwiched POTs $[Cu(dap)(H_2O)_3]_2[\{Cu_8(dap)_4(H_2O)_2\}(B\text{-}\alpha\text{-}SiW_9O_{34})_2]\cdot 6H_2O$ [33] and $[Cu(H_2O)_2]H_2[Cu_8(dap)_4(H_2O)_2(B\text{-}\alpha\text{-}XW_9O_{34})_2]$ ($X = Si^{IV}/Ge^{IV}$) [34] have been reported by us. As a part of our recent work, herein, we report seven inorganic–organic composite POTs constructed from in-situ generated monocopper^{II}-substituted Keggin polyoxoanions and copper^{II}–organoamine complexes: $[Cu(en)_2(H_2O)]_2\{[Cu(en)_2][\alpha\text{-}PW_{11}CuClO_{39}]\}\cdot 3H_2O$ (**1**), $\{[Cu(en)_2(H_2O)][Cu(en)_2]_2[\alpha\text{-}PCuW_{11}O_{39}Cl]\}\cdot 6H_2O$ (**2**), $\{[Cu(en)_2(H_2O)]_2[Cu(en)_2][\alpha\text{-}SiCuW_{11}O_{39}]\}\cdot 5H_2O$ (**3**), $\{[Cu(en)_2(H_2O)]_2[Cu(en)_2][\alpha\text{-}GeCuW_{11}O_{39}]\}\cdot 5H_2O$ (**4**), $\{[Cu(deta)(H_2O)_2]_2[Cu(deta)(H_2O)][\alpha\text{-}GeCuW_{11}O_{39}]\}\cdot 5\ H_2O$ (**5**), $\{[Cu(deta)(H_2O)_2]_2[Cu(deta)(H_2O)][\alpha\text{-}SiCuW_{11}O_{39}]\}\cdot 5H_2O$ (**6**) and $[Cu(dap)_2]_2\{[Cu(dap)_2]_2[Cu(dap)_2][\alpha\text{-}PCuW_{11}O_{39}]_2\}$ (**7**). Their common structural features are that they all contain monocopper^{II}-substituted α-Keggin polyoxoanions as fundamental building units, on which copper^{II}–organoamine complexes are supported as pendants. **1** adopts an isolated structure, in which one five-coordinate $[Cu(en)_2]^{2+}$ cation links to the $[\alpha\text{-}PCuW_{11}O_{39}Cl]^{6-}$ polyoxoanion through a chloride bridge and two five-coordinate $[Cu(en)_2(H_2O)]^{2+}$ cations as charge balance ions are free, whereas **2** utilizes a 1-D chain built by $[\alpha\text{-}PCuW_{11}O_{39}Cl]^{6-}$ polyoxoanions through $[Cu(en)_2]^{2+}$ bridges, in which five-coordinate $[Cu(en)_2]^{2+}$ and six-coordinate $[Cu(en)_2(H_2O)]^{2+}$ cations as pendants bind to the surface of polyoxoanions. Note that **2** is almost identical to the reported $[\{Cu(en)_2\}_3(\alpha\text{-}PCuW_{11}O_{39}Cl)]\cdot 6H_2O$ [21], however, in order to compare the structural relation between **1** and **2**, the synthesis and structure of **2** are also discussed herein. **3–6** contain 1-D linear chains based on $[\alpha\text{-}XCuW_{11}O_{39}]^{6-}$ ($X = Si^{IV}/Ge^{IV}$) polyoxoanions in the pattern of –*A*–*A*–*A*–(*A* = $[\alpha\text{-}XCuW_{11}O_{39}]^{6-}$), while, most interestingly, **7** reveals the first 1-D zigzag chain constructed from $[\alpha\text{-}PCuW_{11}O_{39}]_2^{10-}$ dimeric polyoxoanions via $[Cu(en)_2]^{2+}$ bridges in the pattern of –*A*–*B*–*A*–*B*– (*A* = $[\alpha\text{-}PCuW_{11}O_{39}]_2^{10-}$, *B* = $[Cu(en)_2]^{2+}$). It should be noteworthy that the successful syntheses of **1**–**7** provide some experimental evidences that di-/tri-/hexa-vacant polyoxoanions can be transformed into mono-vacant Keggin polyoxoanions under hydrothermal conditions.

2. Experimental

2.1. Materials and physical measurements

$Na_9[A\text{-}\alpha\text{-}PW_9O_{34}]\cdot 7H_2O$ [35], $K_{12}[\alpha\text{-}H_2P_2W_{12}O_{48}]\cdot 24H_2O$ [36], $K_8[\gamma\text{-}SiW_{10}O_{36}]\cdot 12H_2O$ [37], and $K_8Na_2[A\text{-}\alpha\text{-}GeW_9O_{34}]\cdot 25H_2O$ [38] were synthesized as described in literatures and their purities were identified by IR spectra. Other chemical reagents were used as commercially purchased without further purification. C, H and N elements were determined on a Vario EL III elemental analyzer. Infrared spectra for solid samples were obtained as KBr pellets on an ABB Bomen MB 102 FT-IR spectrometer in the range of 4000–400 cm^{-1}. Thermogravimetric analyses were performed on a Mettler TGA/SDTA851 thermal analyzer in the flowing air atmosphere with a heating rate of 10 °C min^{-1} in the temperature region of 30–1000 °C. ESR spectra were recorded at room temperature and at 77 K on a Bruker ER200-D-SRC spectrometer operating at X-band (9.4 GHz).

2.2. Synthesis of compounds 1 and 2

2.2.1. Synthesis of $[Cu(en)_2(H_2O)]_2\{[Cu(en)_2][\alpha\text{-}PW_{11}CuClO_{39}]\}\cdot 3H_2O$ (*1*)

$Na_9[A\text{-}\alpha\text{-}PW_9O_{34}]\cdot 7H_2O$ (0.246 g, 0.094 mmol) and $CuCl_2\cdot 2H_2O$ (0.128 g, 0.75 mmol) were suspended in H_2O (5 mL), to which ethylenediamine (0.10 mL, 1.480 mmol) and glacial acetic acid (0.05 mL, 0.874 mmol) were added under stirring. The resulting mixture was stirred for 4 h, sealed in a Teflon-lined stainless steel autoclave (20 mL), kept 80 °C for 5 days and then cooled to room temperature. Blue prismatic crystals along with amorphous powders were filtered, washed with distilled water and dried in air at ambient temperature. The crystals were collected mechanically. Yield: ca. 23% (based on $Na_9[A\text{-}\alpha\text{-}PW_9O_{34}]\cdot 7H_2O$). Anal. calc. (%) for: C, 4.22; H, 1.71; N, 4.92. Found (%): C, 4.03; H, 1.85; N, 4.84.

2.2.2. Synthesis of $\{[Cu(en)_2(H_2O)][Cu(en)_2]_2[\alpha\text{-}PCuW_{11}O_{39}Cl]\}\cdot 6H_2O$ (*2*)

A mixture of $K_{12}[\alpha\text{-}H_2P_2W_{12}O_{48}]\cdot 24H_2O$ (0.182 g, 0.046 mmol), $CuCl_2\cdot 2H_2O$ (0.085 g, 0.50 mmol) and ethylenediamine (0.10 mL, 1.480 mmol), glacial acetic acid (0.15 mL, 2.622 mmol) and H_2O (5 mL) was stirred for 3 h, sealed in a Teflon-lined stainless steel autoclave (20 mL), kept at 80 °C for 5 days and then cooled to ambient temperature. Blue prism crystals were obtained by filtration, washed with distilled water and dried in air. Yield: ca. 27% (based on $K_{12}[\alpha\text{-}H_2P_2W_{12}O_{48}]\cdot 24H_2O$). Anal. calcd. (%): C, 4.17; H, 1.81; N, 4.87. Found: C, 3.98; H, 1.92; N, 4.72.

2.2.3. Synthesis of $\{[Cu(en)_2(H_2O)]_2[Cu(en)_2][\alpha\text{-}SiCuW_{11}O_{39}]\}\cdot 5H_2O$ (*3*)

$K_8[\gamma\text{-}SiW_{10}O_{36}]\cdot 12H_2O$ (0.149 g, 0.05 mmol), $CuCl_2\cdot 2H_2O$ (0.128 g, 0.750 mmol), ethylenediamine (0.05 mL, 0.740 mmol) and K_2CO_3 (0.05 mL, 2.0 mol L^{-1}) were suspended in H_2O (5 mL). After stirring for 1.5 h, the mixture was sealed in a Teflon-lined stainless steel autoclave (20 mL), kept at 100 °C for 5 days and then cooled to room temperature. Blue needle crystals were obtained by filtration, washed with distilled water and dried in air. Yield: ca. 50% (based on $K_8[\gamma\text{-}SiW_{10}O_{36}]\cdot 12H_2O$). Anal. calcd. (%): C, 4.22; H, 1.83; N, 4.92. Found: C, 4.04; H, 1.91; N, 4.77.

2.2.4. Synthesis of $\{[Cu(en)_2(H_2O)]_2[Cu(en)_2][\alpha\text{-}GeCuW_{11}O_{39}]\}\cdot 5H_2O$ (*4*)

A mixture of $K_8Na_2[A\text{-}\alpha\text{-}GeW_9O_{34}]\cdot 25H_2O$ (0.154 g, 0.05 mmol), $CuCl_2\cdot 2H_2O$ (0.170 g, 1.000 mmol) and ethylenediamine (0.10 mL, 1.480 mmol) and H_2O (10 mL) was adjusted to pH = 4.5 using glacial acetic acid, stirred for 1.5 h, sealed in a Teflon-lined stainless steel autoclave (20 mL), held at 100 °C for 5 days and then cooled to room temperature. Blue needle crystals were obtained by filtering, washed with distilled water and dried. Yield: ca. 21% (based on $K_8Na_2[A\text{-}\alpha\text{-}GeW_9O_{34}]\cdot 25H_2O$). Anal. calcd. (%): C, 4.17; H, 1.81; N, 4.86. Found: C, 4.02; H, 1.88; N, 4.75.

2.2.5. Synthesis of {[Cu(deta)(H_2O)$_2$]$_2$[Cu(deta)(H_2O)][α-$GeCuW_{11}O_{39}$]} · 5H_2O (**5**)

The analogous way was used for **3** with a mixture of K_8Na_2[*A*-α-GeW_9O_{34}] · 25H_2O (0.246 g, 0.08 mmol), $CuCl_2 \cdot 2H_2O$ (0.213 g, 1.250 mmol), diethylene triamine (0.10 mL, 0.093 mmol), K_2CO_3 (0.05 mL, 2 mol L^{-1}) and H_2O (5 mL). Yield: ca. 28% (based on K_8Na_2[*A*-α-GeW_9O_{34}] · 25 H_2O). Anal. calcd. (%): C, 4.16; H, 1.72; N, 3.64. Found: C, 3.98; H, 1.84; N, 3.57.

2.2.6. Synthesis of {[Cu(deta)(H_2O)$_2$]$_2$[Cu(deta)(H_2O)][α-$SiCuW_{11}O_{39}$]} · 5H_2O (**6**)

The analogous way was used for **3** with the replacement of ethylenediamine with diethylenetriamine (0.05 mL, 0.047 mmol). Yield: ca. 34% (based on K_8[γ-$SiW_{10}O_{36}$] · 12H_2O). Anal. calcd. (%): C, 4.22; H, 1.74; N, 3.69. Found: C, 4.09; H, 1.85; N, 3.62.

2.2.7. Synthesis of [Cu(dap)$_2$]$_2${[Cu(dap)$_2$]$_2$[Cu(dap)$_2$][α-$PCuW_{11}O_{39}$]$_2$} (**7**)

A mixture of Na_9[*A*-α-PW_9O_{34}] · 7H_2O (0.246 g, 0.094 mmol), $CuCl_2 \cdot 2H_2O$ (0.170 g, 1.000 mmol), 1,2-diaminopropane (0.10 mL, 1.178 mmol) and H_2O (5 mL) was stirred for 3.5 h, sealed in a Teflon-lined stainless steel autoclave (20 mL), kept at 160 °C for 5 days, and then cooled to room temperature. Brown prismatic crystals were obtained. Yield: ca. 37% (Based on Na_9[*A*-α-PW_9O_{34}] · 7H_2O). Anal. calcd. (%): C, 5.51; H, 1.54; N, 4.28. Found: C, 5.42; H, 1.71; N, 4.25.

2.3. X-ray structure determination

Intensity data were collected at 293 K on a Rigaku Mercury 70 CCD diffractometer for **1**, **4**, **5** and **7**, a Rigaku Saturn 70 CCD diffractometer for **2** and **3**, and a Siemens Smart 1 K CCD for **6** with graphite-monochromated Mo*K*α radiation ($\lambda = 0.71073$ Å). Cell constants and the orientation matrixes for data collection were obtained from the least-squares refinements of the setting angles in the range of $2.08 \leqslant \theta \leqslant 27.48^\circ$ for **1**, **4**, **5** and **7**, $2.65 \leqslant \theta \leqslant 27.48^\circ$ for **2** and **3** and $1.28^\circ \leqslant \theta \leqslant 25.73^\circ$ for **6**. Lorentz polarization and empirical absorption corrections were applied. The structures were determined and the heavy atoms were found by direct methods and refined by full-matrix least squares using the SHELXL-97 program [39]. The remaining atoms were found after the successive Fourier syntheses. For **1–6**, the anisotropic thermal parameters were refined for all non-hydrogen atoms. In **5** and **6**, the W1 and Cu4 positions are simultaneously statistically occupied by copper^{II} and tungsten^{VI} elements with half occupancy for each, resulting in one expected copper^{II} ion per Keggin cage on the charge balance and crystallographic considerations, which is not uncommon in POM chemistry [40]. For **7**, all non-hydrogen atoms were refined anisotropically with an exception for C4 and C15 atoms, which were only refined isotropically. The hydrogen atoms attached to carbon and nitrogen atoms were geometrically placed. All hydrogen atoms were refined isotropically as the riding atoms using the default SHELXL parameters. Experimental details of crystal structural determinations of **1–7** are presented in Table 1. CCDC 656525–656531 for **1–7** contain the crystallographic data for this paper. These data can obtained free of charge via www.ccdc.cam.ac.uk/data_request/cif or from The Cambridge Crystallographic Data Centre, 12 Union Road, Cambridge CB2 1EZ, UK (Fax: +44-1223-336033; e-mail: deposit@ccdc.cam.ac.uk).

3. Results and discussion

3.1. Synthesis

The hydrothermal method has developed as a routine method in the preparation of a large number of novel inorganic–organic composite solid materials. Aluminosilicate zeolites perhaps represent the well-known group of materials thus prepared [41]. An important feature on the hydrothermal method is that the reaction tends to shift from the thermodynamic to the kinetic so that equilibrium phases are replaced by structurally more complicated metastable phases, directly leading to novel compounds with unexpected topologies and properties. Although a great number of purely inorganic *d*-electron TM encapsulated POMs, especially for lacunary Keggin- and Dawson-type POT derivatives, have been obtained using di-, tri- or multi-vacant POM precursors by virtue of conventional aqueous solution methods under the atmosphere pressure, the research system containing di-/tri-/hexa-vacant POM precursors and TM salts in the presence of organoamines remain less explored under hydrothermal conditions to date. As a part of our continuous efforts in the construction of inorganic–organic hybrid solid materials [42–44], we are currently interested in the branch project containing lacunary POM precursors and copper^{II} cations to synthesize unique POTs in the presence of organoamines under hydrothermal conditions. Here, organoamines were chosen for their ability to chelate copper^{II} cations leaving two trans-located free positions so that the resulting copper^{II}–organoamine complexes can act as the bridging agents to connect adjacent POMs generating novel extended architectures [21]. In our search, besides some hexa- or octa-Cu^{II}-substituted trivacant Keggin POM derivatives [32–34], we also obtained seven new inorganic–organic composite POTs **1–7**. Systematic synthetic investigation elucidates that the final products are strongly dependent on the ratio of copper^{II} salts/lacunary POM precursors, the tuneable role of different organoamines and temperature.

1 and a 3-D hexa-Cu^{II}-substituted POT [Cu_6(en)$_3$(H_2O)$_3$(OH)$_3$][*B*-α-PW_9O_{34}] · 7H_2O [33] were separated from the hydrothermal reaction of $CuCl_2 \cdot 2H_2O$, Na_9[*A*-α-PW_9O_{34}] · 7H_2O and en at 80 °C for 5 days by varying the Cu^{2+}/[*A*-α-PW_9O_{34}]$^{9-}$ ratio. Moreover, when the temperature varied in the range of 80–140 °C, both could be still isolated, however, when the temperature was higher than 170 °C, both could not be obtained, which may be related to the decomposition of the [*A*-α-PW_9O_{34}]$^{9-}$ polyoxoanion at the higher temperature. Additionally, when the Cu^{2+}/[*A*-α-PW_9O_{34}]$^{9-}$/en ratio equalled to 0.5/0.05/1.48 in 10 mL H_2O at 80 °C with pH = 4.5 adjusted by glacial acetic acid, a reported 1-D chain-like compound based on [α-$PW_{11}CuO_{39}$]$^{5-}$ polyoxoanions was isolated (its cell constants: orthorhombic, *Cmc*2$_1$, a = 10.8907(8) Å, b = 48.723(3) Å, c = 20.1238(14) Å, V = 10678.3 (13) Å^3) [21], but its detail structure cannot be solved by Dolbecq et al. and by us because of the very poor quality of the crystals. However, our starting materials ([*A*-α-PW_9O_{34}]$^{9-}$), pH (4.5) and temperature (80 °C) are rather different from those reported by Dolbecq et al. ($Na_2WO_4 \cdot 2H_2O$, pH = 11.5 and 160 °C). Subsequently, when replacing en with dap in this system at 160 °C, another novel 1-D zigzag chain-like phosphotungstate **7** was separated. When Na_{10}[*A*-α-SiW_9O_{34}] · 18H_2O [45] reacted with $CuCl_2 \cdot 2H_2O$ at 100 °C in the presence of en or dap, three octa-Cu^{II} sandwiched silicotungstates [H_2en]$_2$[Cu_8(en)$_4$(H_2O)$_2$(*B*-α-SiW_9O_{34})$_2$] · 8H_2O [46], [Cu(dap)(H_2O)$_3$]$_2$[Cu_8(dap)$_4$(H_2O)$_2$(*B*-α-SiW_9O_{34})$_2$] · 6H_2O [33] and Cu(H_2O)$_2$[Cu_8(dap)$_4$(H_2O)$_2$(*B*-α-SiW_9O_{34})$_2$ [34] were obtained. At 160 °C, we also found a reported compound [Cu(en)$_2$(H_2O)]{[Cu(en)$_2$][α-$SiCuW_{11}O_{39}$]} · 7H_2O [21]. When the [*A*-α-GeW_9O_{34}]$^{10-}$/Cu^{2+}/organoamine system was developed, two new 1-D monocopper^{II}-substituted Keggin

Table 1
Crystal data and structure refinement parameters for **1–7**

	1	**2**	**3**	**4**
Empirical formula	$C_{12}H_{58}N_{12}O_{44}ClCu_4P\ W_{11}$	$C_{12}H_{62}N_{12}O_{46}ClCu_4P\ W_{11}$	$C_{12}H_{62}N_{12}O_{46}Cu_4Si\ W_{11}$	$C_{12}H_{62}N_{12}O_{46}Cu_4Ge\ W_{11}$
Formula weight	3417.63	3453.67	3415.34	3459.84
Crystal system	Monoclinic	Monoclinic	Triclinic	Triclinic
Space group	*P*2(1)/*c*	*P*2(1)/*n*	*P*1	*P*1
a (Å)	13.941(2)	12.6823(19)	10.962(3)	10.9791(12)
b (Å)	13.804(2)	21.524(4)	12.323(3)	12.3409(14)
c (Å)	30.611(5)	22.453(4)	12.780(3)	12.8033(15)
α (deg)	90	90	101.837(2)	101.831(4)
β (deg)	90.246(3)	95.689(3)	110.433(2)	110.414(2)
γ (deg)	90	90	107.64	107.6530(10)
V (Å^3)	5891.2(17)	6098.9(17)	1445.3(7)	1452.4(3)
Z	4	4	1	1
D_c (g cm^{-3})	3.853	3.761	3.924	3.956
Absorption coefficient (mm^{-1})	22.966	22.189	23.354	23.727
T (K)	293(2)	293(2)	293(2)	293(2)
Limiting indices	$-15\leqslant h\leqslant 16$	$-11\leqslant h\leqslant 15$	$-14\leqslant h\leqslant 14$	$-12\leqslant h\leqslant 13$
	$-16\leqslant k\leqslant 15$	$-25\leqslant k\leqslant 21$	$-15\leqslant k\leqslant 15$	$-14\leqslant k\leqslant 14$
	$-33\leqslant l\leqslant 36$	$-26\leqslant l\leqslant 26$	$-11\leqslant l\leqslant 16$	$-15\leqslant l\leqslant 11$
No. of reflections collected	35,887	36,546	11,232	9036
No. of independent reflections	10,218	10,625	8291	6681
Data/restrains/parameters	10,218/6/766	10,625/6/784	8291/67/775	6681/96/776
Goodness-of-fit on F^2	1.074	1.091	0.895	1.012
Final *R* indices [$I>2\sigma(I)$]	$R_1=0.0443$[a]	$R_1=0.0423$	$R_1=0.0313$	$R_1=0.0435$
	w$R_2=0.1077$[b]	w$R_2=0.1068$	w$R_2=0.0615$	w$R_2=0.0974$
R indices (all data)	$R_1=0.0508$	$R_1=0.0469$	$R_1=0.0345$	$R_1=0.0510$
	w$R_2=0.1122$	w$R_2=0.1098$	w$R_2=0.0619$	w$R_2=0.1024$
	5	**6**	**7**	
Empirical formula	$C_{12}H_{59}N_9O_{49}Cu_4GeW_{11}$	$C_{12}H_{59}N_9O_{49}Cu_4SiW_{11}$	$C_{30}H_{100}N_{20}O_{78}Cu_7P_2W_{22}$	
Formula weight	3462.78	3418.28	6540.72	
Crystal system	Monoclinic	Monoclinic	Monoclinic	
Space group	*P*2(1)/*n*	*P*2(1)/*n*	*P*2(1)/*c*	
a (Å)	11.078(4)	11.1309(2)	13.1424(7)	
b (Å)	22.892(7)	22.8491(3)	38.3930(18)	
c (Å)	22.499(7)	22.5174(5)	12.2522(6)	
α (deg)	90	90	90	
β (deg)	97.979(4)	97.9380(10)	110.481(2)	
γ (deg)	90	90	90	
V (Å^3)	5650(3)	5672.00(18)	5791.4(5)	
Z	4	4	2	
D_c (g cm^{-3})	4.071	4.003	3.751	
Absorption coefficient (mm^{-1})	24.398	23.806	23.125	
T (K)	293(2)	293(2)	293(2)	
Limiting indices	$-13\leqslant h\leqslant 13$	$-13\leqslant h\leqslant 13$	$-15\leqslant h\leqslant 13$	
	$-27\leqslant k\leqslant 27$	$-27\leqslant k\leqslant 22$	$-44\leqslant k\leqslant 45$	
	$-19\leqslant l\leqslant 26$	$-18\leqslant l\leqslant 27$	$-13\leqslant l\leqslant 14$	
No. of reflections collected	33,317	28,258	33,423	
No. of independent reflections	9765	10,701	10,067	
Data/restrains/parameters	9765/108/776	10,701/66/776	0067/13/708	
Goodness-of-fit on F^2	1.148	1.102	1.111	
Final *R* indices [$I>2\sigma(I)$]	$R_1=0.0836$	$R_1=0.0709$	$R_1=0.0532$	
	w$R_2=0.1749$	w$R_2=0.1464$	w$R_2=0.1158$	
R indices (all data)	$R_1=0.1051$	$R_1=0.0991$	$R_1=0.0640$	
	w$R_2=0.1854$	w$R_2=0.1594$	w$R_2=0.1216$	

[a] $R_1=\sum||F_o|-|F_c||/\sum|F_o|$.
[b] $wR_2=[\sum w(F_o^2-F_c^2)^2/\sum w(F_o^2)^2]^{1/2}$; $w=1/[\sigma^2(F_o^2)+(xP)^2+yP]$, $P=(F_o^2+2F_c^2)/3$, where $x=0.0592$, $y=0.0000$ for **1**, $x=0.0537$, $y=73.8252$ for **2**, $x=0.0129$, $y=0.0000$ for **3**, $x=0.0523$, $y=0.0000$ for **4**, $x=0.0526$, $y=406.5601$ for **5**, $x=0.0266$, $y=836.7985$ for **6** and $x=0.0442$, $y=100.2505$ for **7**.

germanotungstates **4** and **5** were successively separated at 100 °C besides two octa-Cu^{II} sandwiched POTs $H_4\{[Cu_8(dap)_4(H_2O)_2(B\text{-}\alpha\text{-}GeW_9O_{34})_2]\cdot 13H_2O$ [47] and $Cu(H_2O)_2[Cu_8(dap)_4(H_2O)_2(B\text{-}\alpha\text{-}GeW_9O_{34})_2$ [34]. When $K_8[\gamma\text{-}SiW_{10}O_{36}]\cdot 12H_2O$ was used to react with $CuCl_2\cdot 2H_2O$, **3** and **6** were afforded. It is of interest that the reaction of $K_8[\gamma\text{-}SiW_{10}O_{36}]\cdot 12H_2O$ with $CuCl_2\cdot 2H_2O$ at 100 °C can also lead to two aforementioned octa-Cu^{II} sandwiched silicotungstates $[H_2en]_2[Cu_8(en)_4(H_2O)_2(B\text{-}\alpha\text{-}SiW_9O_{34})_2]\cdot 8H_2O$ [46] and $[Cu(dap)(H_2O)_3]_2[Cu_8(dap)_4(H_2O)_2(B\text{-}\alpha\text{-}SiW_9O_{34})_2]\cdot 6H_2O$ [33]. In addition, **3** and **4** could be also synthesized under similar conditions by the hydrothermal reaction of $K_8[\alpha\text{-}SiW_{11}O_{39}]\cdot 13H_2O$ [37] or $K_6Na_2[\alpha\text{-}GeW_{11}O_{39}]\cdot 13H_2O$ [48] with $CuCl_2\cdot 2H_2O$ in the presence of en. Later, $K_{12}[\alpha\text{-}H_2P_2W_{12}O_{48}]\cdot 24H_2O$ was introduced to react with $CuCl_2\cdot 2H_2O$ in the presence of en at 80 °C, to our great surprise, a 1-D monocopper^{II}-substituted α-Keggin tungstophosphate **2** and a 1-D α_1-mono-vacant Dawson tungstophosphate $(H_2en)_{0.5}H[Cu(en)_2(H_2O)]_2\{[Cu(en)_2](\alpha_1\text{-}P_2CuW_{17}O_{61})\}\cdot 8H_2O$ [49] were simultaneously obtained by changing initial concentrations of $K_{12}[\alpha\text{-}H_2P_2W_{12}O_{48}]\cdot 24H_2O$ and $CuCl_2\cdot 2H_2O$. However, when we

use 1,3-diaminopropane, 1,6-diaminohexane, triethylenetetramine or tetraethylenepentamine in place of en, dap or deta in the studied systems, only amorphous powders were afforded. These explorations elucidate that organoamines play an important tuneable role in the formation and structural construction of these POTs.

It is noteworthy that **1–7** all experienced transformations of different lacunary polyoxoanions (Fig. 1). In the case of **1**, **7** and $[Cu_6(en)_3(H_2O)_3(OH)_3][B\text{-}\alpha\text{-}PW_9O_{34}]\cdot 7H_2O$ [33], we synchronously observed transformations of $[A\text{-}\alpha\text{-}PW_9O_{34}]^{9-}\rightarrow[\alpha\text{-}PW_{11}O_{39}]^{7-}$ for **1** and **7**, and $[A\text{-}\alpha\text{-}PW_9O_{34}]^{9-}\rightarrow[B\text{-}\alpha\text{-}PW_9O_{34}]^{9-}$ for the hexa-Cu^{II}-substituted POT. In the formation of **4**, **5,** $[Cu(en)_2(H_2O)]\{[Cu(en)_2][\alpha\text{-}SiCuW_{11}O_{39}]\}\cdot 7H_2O$ [21] and those octa-Cu^{II} sandwiched trivacant Keggin POTs, transformations of $[\alpha\text{-}A\text{-}XW_9O_{34}]^{10-}\rightarrow[\alpha\text{-}XW_{11}O_{39}]^{8-}$ and $[A\text{-}\alpha\text{-}XW_9O_{34}]^{10-}\rightarrow[B\text{-}\alpha\text{-}XW_9O_{34}]^{10-}$ ($X=Ge^{IV}$ or Si^{IV}) were also observed (Fig. 1a). The similar isomerizations of $[A\text{-}\alpha\text{-}XW_9O_{34}]^{9/10-}\rightarrow[B\text{-}\alpha\text{-}XW_9O_{34}]^{9/10-}$ ($X=P^{V}$, Ge^{IV} or Si^{IV}) were previously encountered [37,50–54]. For example, in 2004, when Kortz et al. reacted the $[A\text{-}\alpha\text{-}GeW_9O_{34}]^{10-}$ anion with Cu^{2+}, Mn^{2+}, Zn^{2+} and Cd^{2+} ions to construct sandwich-type germanotungstates $[M_4(H_2O)_2(B\text{-}\alpha\text{-}GeW_9O_{34})_2]^{12-}$, they already observed the occurrence of the isomerization of $[A\text{-}\alpha\text{-}GeW_9O_{34}]^{10-}\rightarrow[B\text{-}\alpha\text{-}GeW_9O_{34}]^{10-}$ in the aqueous acidic medium upon heating [50]. Additionally, Knoth et al. [51] demonstrated that the $[A\text{-}\alpha\text{-}PW_9O_{34}]^{9-}$ anion can be transformed to the $[B\text{-}\alpha\text{-}PW_9O_{34}]^{9-}$ anion in solution in the presence of the first-row transition-metal ions upon heating. Domaille [35] showed that the same isomerization could be accomplished in the solid state. Later, Kortz also observed this isomerization when the $[A\text{-}\alpha\text{-}PW_9O_{34}]^{9-}$ anion reacted with the Ni^{2+} ion to prepare $[Ni_3Na(H_2O)_2(PW_9O_{34})_2]^{11-}$ in 2002 [53]. Recently, when we prepared hexa-Ni^{II} substituted POTs $[[Ni(L)_2]_m[\{Ni_6(\mu_3\text{-}OH)_3(L)_{3-n}(H_2O)_{6+2n}\}(B\text{-}\alpha\text{-}XW_9O_{34})]\cdot yH_2O$ (L = organodiamines, $X=P^{V}/Si^{IV}$) [33], transformations of $[A\text{-}\alpha\text{-}PW_9O_{34}]^{9-}\rightarrow[B\text{-}\alpha\text{-}PW_9O_{34}]^{9-}$ and $[A\text{-}\alpha\text{-}SiW_9O_{34}]^{10-}\rightarrow[B\text{-}\alpha\text{-}SiW_9O_{34}]^{10-}$ were observed under hydrothermal conditions. Furthermore, in the preparation of organometallic derivatives of trivacant Keggin POMs, the isomerization of $[B\text{-}\alpha\text{-}PW_9O_{34}]^{9-}\rightarrow[A\text{-}\alpha\text{-}PW_9O_{34}]^{9-}$ also occurred when grafting organometallic groups onto the POM surface [55–57]. For example, the fixation of RPO^{2+} (R = Et, Bu^n, Bu^t and Ph) groups onto the lacunae of the $[B\text{-}\alpha\text{-}PW_9O_{34}]^{9-}$ induced the isomerization of $[B\text{-}\alpha\text{-}PW_9O_{34}]^{9-}\rightarrow[A\text{-}\alpha\text{-}PW_9O_{34}]^{9-}$ [55], which was also observed for its organosilyl derivatives [56,57]. In the formation of **3**, **6** and two octa-Cu^{II} sandwiched silicotungstates, we observed that the $[\gamma\text{-}SiW_{10}O_{36}]^{8-}$ anion could be transformed to the $[\alpha\text{-}SiW_{11}O_{39}]^{8-}$ or $[B\text{-}\alpha\text{-}SiW_9O_{34}]^{10-}$ anion under hydrothermal conditions (Fig. 1b). The isomerization of $[\gamma\text{-}SiW_{10}O_{36}]^{8-}\rightarrow[B\text{-}\alpha\text{-}SiW_9O_{34}]^{10-}$ was constantly encountered in silicotungstate chemistry [58,59]. Tézé and Hervé [37] have systematically studied transformations between lacunary Keggin silicotungstate polyoxoanions. Interaction of the metastable $[\gamma\text{-}SiW_{10}O_{36}]^{8-}$ anion with TM ions led to a series of mono-, di- and tri-TM-substituted POM species [60–64]. Interestingly, although the hexa-vacant $[\alpha\text{-}H_2P_2W_{12}O_{48}]^{12-}$ polyoxoanion could be transformed to the plenary $[\alpha\text{-}P_2W_{18}O_{62}]^{6-}$ and α_2-mono-vacant $[\alpha_2\text{-}P_2W_{17}O_{61}]^{10-}$ polyoxoanions in the previous study [65], transformations of $[\alpha\text{-}H_2P_2W_{12}O_{48}]^{12-}\rightarrow[\alpha\text{-}PW_{11}O_{39}]^{7-}$ and $[\alpha\text{-}H_2P_2W_{12}O_{48}]^{12-}\rightarrow[\alpha_1\text{-}P_2W_{17}O_{61}]^{10-}$ were firstly observed in our findings (Fig. 1c). From the above analysis, although there were some reports on transformations between tri- and di-vacant Keggin polyoxoanions, investigations on transformations between di-/tri-/hexa-vacant polyoxoanions and mono-vacant Keggin polyoxoanions were very rare. In summary, the successful syntheses of **1–7** provide some experimental evidences that di-/tri-/hexa-vacant polyoxoanions can be transformed into mono-vacant Keggin polyoxoanions under hydrothermal conditions.

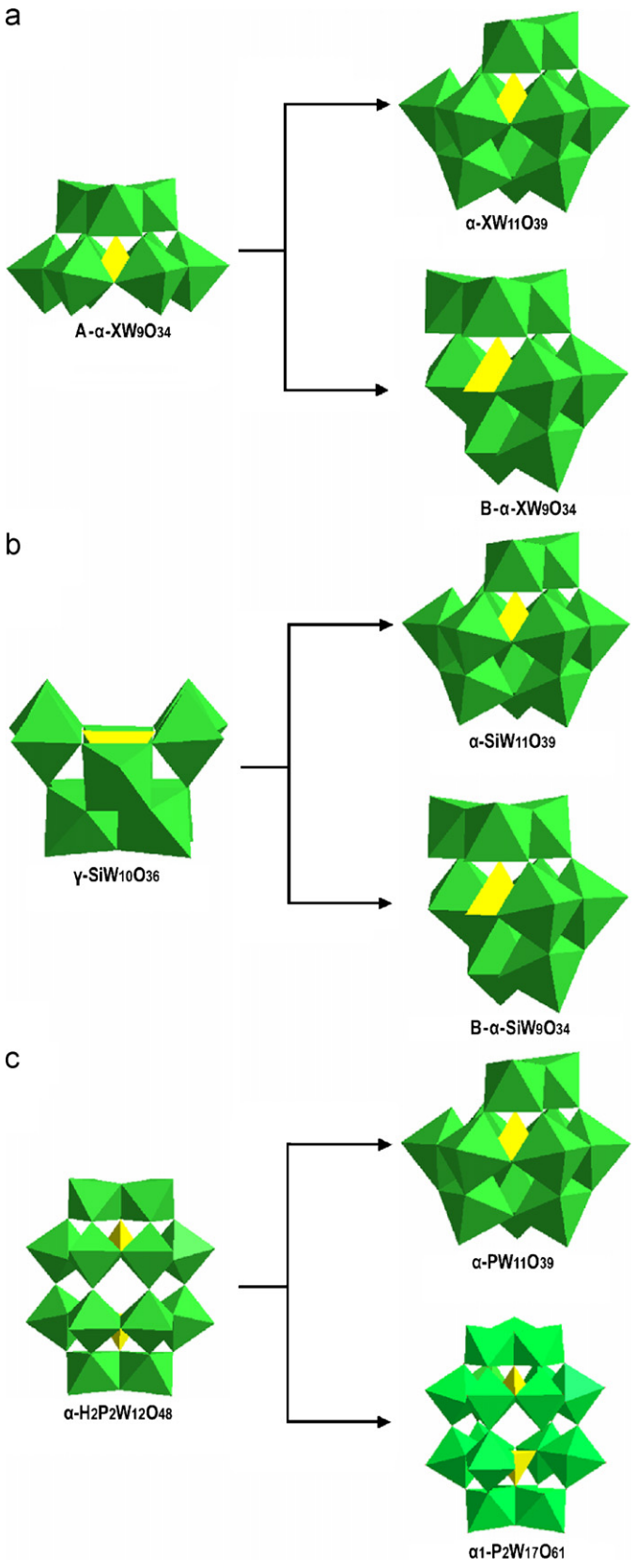

Fig. 1. The transformation relationships between different lacunary polyoxoanions used in the present paper ($X=P^{V}$, Si^{IV} or Ge^{IV}).

3.2. Structural description

Compounds **1–7** were prepared by exploitation of the hydrothermal reaction of $CuCl_2 \cdot 2H_2O$ and suitable lacunary POM precursors $Na_9[A\text{-}\alpha\text{-}PW_9O_{34}] \cdot 7H_2O$, $K_8[\gamma\text{-}SiW_{10}O_{36}] \cdot 12H_2O$, $K_8Na_2[A\text{-}\alpha\text{-}GeW_9O_{34}] \cdot 25H_2O$ or $K_{12}[\alpha\text{-}H_2P_2W_{12}O_{48}] \cdot 24H_2O$ in the presence of organoamines at appropriate temperature for 5 days. Although the reactants are somewhat different, the common structural features of **1–7** are that they all consist of monocopper^{II}-substituted α-Keggin polyoxoanions as fundamental building units, on which copper^{II}–organoamine complexes are supported as pendants. As we know, the $[\alpha\text{-}XW_{11}O_{39}]^{7/8-}$ monovacant polyoxoanion derives from the $[\alpha\text{-}XW_{12}O_{40}]^{3/4-}$ parent polyoxoanion by removal of a $W=O_t$ group. Accordingly, the monocopper^{II}-substituted α-Keggin $[\alpha\text{-}XCuW_{11}O_{39}]^{5/6-}$ subunit derives from the $[\alpha\text{-}XW_{11}O_{39}]^{7/8-}$ synthon by inserting a Cu^{II} ion into the vacant site and can be described as a central XO_4 tetrahedron surrounded by four vertex-sharing M_3O_{13} trimers: one CuW_2O_{13} and three W_3O_{13}. In **1–7**, the W–O bond distances and the O–W–O bond angles are in the range of 1.66(2)–2.509(9) Å and 69.6(3)–175.1(2)°, respectively. Additionally, in the description of crystal structures, the weak Cu–O interactions will be considered because the evident Jahn–Teller distortion of copper^{II} ions in the crystal field leads to the elongation of the Cu–O distances [21,66,67].

The structures of **1** and **2** are intimately relevant. The formula unit of **1** consists of a monocopper^{II}-substituted polyoxoanion $[\alpha\text{-}PCuW_{11}O_{39}Cl]^{6-}$, one coordinated cation $[Cu1(en)_2]^{2+}$, two discrete cations $[Cu2(en)_2(H_2O)]^{2+}$ and $[Cu3(en)_2(H_2O)]^{2+}$ as well as three lattice water (Fig. 2a). Notably, the $[Cu1(en)_2]^{2+}$ cation joins to the polyoxoanion via a chlorine bridge [Cu–Cl = 2.478(4)–2.844(4) Å]. Similarly, the formula unit of **2** is also a monocopper^{II}-substituted polyoxoanion $[\alpha\text{-}PW_{11}CuO_{39}Cl]^{6-}$, to which are linked by three coordinated copper^{II}-en cations $[Cu1(en)_2]^{2+}$, $[Cu2(en)_2(H_2O)]^{2+}$ and $[Cu3(en)_2]^{2+}$ via a chlorine bridge [Cu–Cl = 2.415(4)–2.860(6) Å], a bridging oxygen atom [$Cu–O_b = 2.854(11)$ Å] and a terminal oxygen atom [$Cu–O_t = 2.439(9)$ Å], respectively (Fig. 2b). Interestingly, distinct from **1**, adjacent structural units of **2** are connected together by the $[Cu1(en)_2]^{2+}$ cations through the W3–O11–Cu1–Cl–Cu4 linkers to construct a 1-D linear polymeric chain in the pattern of *–A–B–A–B–* (Fig. 2c). In a word, **1** and **2** provide two rare examples of the monocopper^{II}-substituted POMs where the mono-vacant $[\alpha\text{-}PW_{11}O_{39}]^{7-}$ anion acts as a pentadentate ligand for a $[CuCl]^{+}$ group. So far as we know, the phenomena that the chlorine ion acts as a bridge in connecting TM cations with POM moieties in POM chemistry are very rare [21]. Though the structure of **1** is very similar to those of **2** and $[\{Cu(en)_2\}_3(\alpha\text{-}PCuW_{11}O_{39}Cl)] \cdot 6H_2O$ [21], the evident differences are present: (a) **1** is an isolated structure whereas **2** and $[\{Cu(en)_2\}_3(\alpha\text{-}PCuW_{11}O_{39}Cl)] \cdot 6H_2O$ [21] are a 1-D linear polymeric chain through a $[Cu(en)_2]^{2+}$ bridge via a Cu–Cl–Cu–O–W linkages; (b) the two square pyramidal $[Cu(en)_2(H_2O)]^{2+}$ pendants in **1** are discrete while the square pyramidal $[Cu(en)_2]^{2+}$ and octahedral $[Cu(en)_2(H_2O)]^{2+}$ pendants are bonded to polyoxoanions in **2** and $[\{Cu(en)_2\}_3(\alpha\text{-}PCuW_{11}O_{39}Cl)] \cdot 6H_2O$ [21]; (c) their cell constants are distinct despite they belong to the monoclinic system. Additionally, compound **2** is almost identical to the previously reported $[\{Cu(en)_2\}_3(\alpha\text{-}PCuW_{11}O_{39}Cl)] \cdot 6H_2O$ [21] except that **2** has a coordination water molecule more than $[\{Cu(en)_2\}_3(\alpha\text{-}PCuW_{11}O_{39}Cl)] \cdot 6H_2O$ in a formula unit, however, their synthetic conditions are completely different. **2** was obtained based on $K_{12}[\alpha\text{-}H_2P_2W_{12}O_{48}] \cdot 24H_2O$ while $[\{Cu(en)_2\}_3(\alpha\text{-}PCuW_{11}O_{39}Cl)] \cdot 6H_2O$ was prepared using $Na_2WO_4 \cdot 2H_2O$ and H_3PO_4 as starting materials.

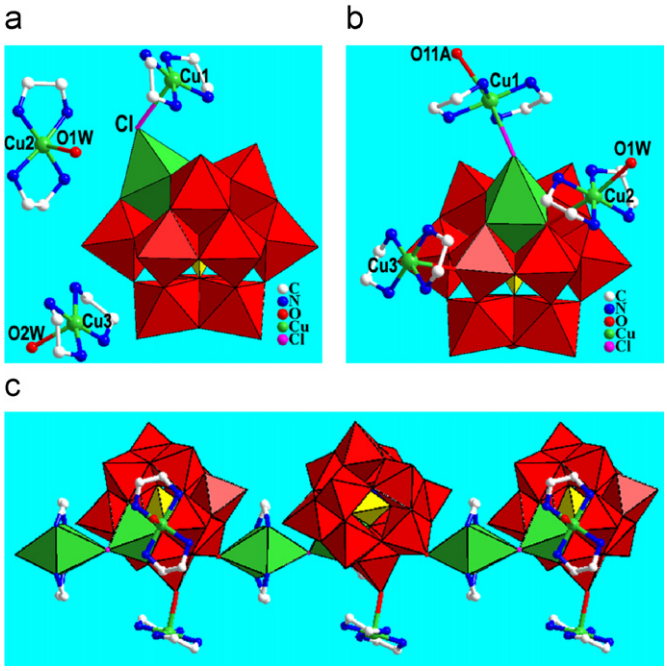

Fig. 2. Combined polyhedral/ball-and-stick representations of the structural units of **1** (a) and **2** (b) with the selected atomic numbering scheme. {WO_6}: red octahedron; {XO_4}: yellow tetrahedron; {CuO_6} in the vacant site: green octahedron. The atom with the suffix A is generated by the symmetry operation: −0.5+*x*, 1.5−*y*, −0.5+*z* for O11A. (c) The 1-D polymeric chain in **2** built by $[\alpha\text{-}PCuW_{11}O_{39}Cl]^{6-}$ polyoxoanions through six-coordinate $[Cu(en)_2]^{2+}$ bridges in the pattern of *–A–B–A–B–*. The hydrogen atoms attached to carbon and nitrogen atoms and lattice water molecules are omitted for clarity. {WO_6}: red octahedron; {XO_4}: yellow tetrahedron; {CuO_6} in the vacant site and {CuO_2N_4} in $[Cu(en)_2]^{2+}$ bridge: green octahedron. For interpretation of the references to colour in this figure legend, the reader is referred to the web version of this article.

The Cu4 atom is perfectly located in the defect site of the polyoxoanion $[\alpha\text{-}PW_{11}O_{39}]^{7-}$ with the $Cu–O_{b,c}$ distances of 1.974(8)–1.999(8) Å for **1** and 1.944(9)–2.023(9) Å for **2**, respectively, and their average distances of 1.981 Å for **1** and 1.976 Å for **2** are longer than the average $W–O_{b,c}$ distance (1.929 Å for **1** and 1.910 Å for **2**), thus the CuO_5Cl octahedra in **1** and **2** are off-centered compared to other WO_6 octahedra and are also axially elongated due to the Jahn–Teller effect, which has been observed in $[\{Cu(en)_2\}_3(\alpha\text{-}PCuW_{11}ClO_{39})] \cdot 6H_2O$ [21]. Besides, in the case of **1**, the two free $[Cu2(en)_2(H_2O)]^{2+}$ and $[Cu3(en)_2(H_2O)]^{2+}$ cations are both five-coordinate and exhibit highly distorted square pyramidal geometry. In both cases, the equatorial plane is defined by four nitrogen atoms from en ligands with Cu–N distances of 1.970(11)–2.038(12) Å, whereas the apical position is occupied by a water molecule with $Cu–O_w$ distances of 2.347(10)–2.348(9) Å. In contrast, as for **2**, the $[Cu2(en)_2(H_2O)]^{2+}$ cation is a distorted octahedral geometry where the equatorial plane is formed by four nitrogen atoms from en ligands with Cu–N distances of 1.998(12)–2.043(12) Å and one water molecule and a bridging oxygen atom occupy the apical positions in the *trans* arrangement with $Cu–O_w$ and $Cu–O_b$ distances of 2.509(11) and 2.854(11) Å, respectively. The $[Cu3(en)_2]^{2+}$ cation adopts a distorted square pyramidal geometry, in which four nitrogen atoms from en ligands sit on the basal plane with Cu–N distances of 1.944(16)–2.018(14) Å and a terminal oxygen atom inhibits in the apical position with the $Cu–O_t$ distance of 2.439(8) Å. In **1**, the P atom resides in the center of a PO_4 tetrahedron, which has been somewhat deformed resulting from the removal of one $[W=O_t]^{4+}$ group and the incorporation of the $[Cu–Cl]^{+}$ group into the backbone of the mono-vacant polyoxoanion. The $P–O_a$ distances vary from 1.527(8) to 1.576(7) Å, which are in approximate accordance with the previous work and the O–P–O bond angles are in the range of 108.8(4)–110.7(4)° [20,21]. The similar

distortions are observed in all the WO_6 octahedra and XO_4 tetrahedra in **2**–**7**.

Compounds **3** and **4** are nearly isostructural except the different heteroatoms in the central cavities (Si^{IV} for **3** and Ge^{IV} for **4**) and both crystallize in the triclinic space group *P*1. Only the structure of **3** is described here. Its structural unit consists of one monocopper^{II}-substitued Keggin polyoxoanion $[\alpha\text{-SiCuW}_{11}O_{39}]^{6-}$, two pendant $[Cu(en)_2(H_2O)]^{2+}$ cations, one pendant $[Cu(en)_2]^{2+}$ cation and five lattice water molecules (Fig. 3a). Adjacent structural units $\{[Cu(en)_2(H_2O)]_2[Cu(en)_2][\alpha\text{-SiCuW}_{11}O_{39}]\}$ are interconnected by sharing terminal oxygen atoms to make the 1-D polymeric linear chain running along the [100] direction (Fig. 3c). Alternatively, the polymeric polyoxoanion chain can be considered as the result of the substitution of a water molecule on a $[\alpha\text{-SiCuW}_{11}(H_2O)O_{39}]^{6-}$ anion by a terminal oxygen atom on a WO_6 octahedron from the adjacent Keggin unit. This common terminal oxygen atom connects two opposite positions of the Keggin units occupied by a Cu^{II} atom and a W^{VI} atom, respectively. This polymeric chain is similar to those of $[ET]_8[PMnW_{11}O_{39}]\cdot 2H_2O$ [18], (ET = bis(ethylenedithio)tetrathiofulvalene), $[NEt_3H]_5[XCoW_{11}O_{39}]\cdot 3H_2O$ ($X = P^V/As^V$) [19], and $K_3[Cu^I(4,4'\text{-bpy})]_3[Si\ Cu^{II}W_{11}O_{39}]\cdot 11H_2O$ [24], where Mn^{II}, Co^{II} and Cu^{II} ions are disordered and $[Co(dpa)_2(OH_2)_2]_2[Hdpa][PCoW_{11}O_{39}]$ (dpa = di-2-pyridylamine) [20], where the Co^{II} ion in the POM core is perfectly localized. The pendant $[Cu1(en)_2(H_2O)]^{2+}$ ion inhibits an octahedral geometry defined by four nitrogen atoms from en ligands [Cu–N: 1.935(17)–2.066(18) Å], one water oxygen atom [Cu–O_w: 2.642(2) Å] and one terminal oxygen atom from the POM unit [Cu–O_t: 2.716(1) Å], and connects to a 'equatorial' WO_6 octahedron on the $[\alpha\text{-SiCuW}_{11}O_{39}]^{6-}$ anion through the terminal oxygen atom, whereas the pendant octahedral $[Cu2(en)_2(H_2O)]^{2+}$ ion links to a 'polar' WO_6 octahedron on a W_3O_{13} trimer with Cu–N, Cu–O_w and Cu–O_t distances of 1.965(16)–2.040(16), 2.317(14) and 2.844(1) Å, respectively. The pendant $[Cu3(en)_2]^{2+}$ ion links to another 'polar' WO_6 octahedron from the same W_3O_{13} trimer and resides in a distorted square pyramid, in which the basic plane is defined by four nitrogen atoms from en ligands with Cu–N distances of 1.977(14)–2.018(16) Å and the axial vertex is occupied by a terminal oxygen atom from the POM unit with Cu–O_t distance of 2.522(1) Å.

The structures of **5** and **6** are also isostructural and very similar to those of **3** and **4**. Both crystallize in the monoclinic space group $P2_1/n$. Only the structure **5** is described here. The structural unit of **5** contains a monocopper^{II}-substituted $[\alpha\text{-GeCuW}_{11}O_{39}]^{6-}$ anion, two crystallographically independent $[Cu(deta)(H_2O)_2]^{2+}$ ions and one $[Cu(deta)(H_2O)]^{2+}$ ion (Fig. 3b). Different from **3** and **4**, the W1 and Cu4 sites of **5** and **6** are simultaneously occupied by the Cu^{II} and W^{VI} atoms with half occupancy for each in two opposite W_3O_{13} trimers of the polyoxoanion $[\alpha\text{-GeCuW}_{11}O_{39}]^{6-}$. This disordered phenomenon has been observed in the previous study [40]. Adjacent structural units are interconnected together by terminal oxygen atoms via Cu/W–O–Cu/W linkers [Cu4–O1 = 2.10(4) Å and W1–O1 = 2.03(3) Å] forming the 1-D infinite linear polymeric chain running along the [100] direction (Fig. 3d). Different from **3** and **4**, the square pyramidal $[Cu2(deta)(H_2O)]^{2+}$ cation grafts onto the $[\alpha\text{-GeCuW}_{11}O_{39}]^{6-}$ polyoxoanion by a bridging oxygen rather than a terminal oxygen atom [Cu–N: 1.94(2)–2.07(3) Å, Cu–O_w: 1.95(2) Å and Cu–O_b: 2.734(1) Å]. This bridging oxygen coordination mode is uncommon in POM chemistry mainly because the nucleophility of bridging oxygen atoms is much lower than that of terminal oxygen atoms. This phenomenon is also observed in **2**, **4** and **7**. Both $[Cu1(deta)(H_2O)_2]^{2+}$ and $[Cu3(deta)(H_2O)_2]^{2+}$ cations have the distorted octahedral coordination geometries constituted by three nitrogen atoms from tridendate deta ligands in the *mer* fashion, two water oxygen atoms and one terminal oxygen atom from the POM unit with Cu–N, Cu–O_w and Cu–O_t distances of 1.99(2)–2.04(2), 2.02(2)–2.33(2) and 2.665(1) Å for the $[Cu1(deta)(H_2O)_2]^{2+}$ cation and 2.01(2)–2.05(2), 2.03(2)–2.42(2) and 2.914 (1) Å for the $[Cu3(deta)(H_2O)_2]^{2+}$ cation.

The 1-D linear structures of **2–6** can be described as a molecular line of $[\alpha\text{-PCuW}_{11}O_{39}Cl]^{6-}$ polyoxoanions by means of connection role of $[Cu(en)_2]^{2+}$ cations for **2** and $[\alpha\text{-}X\text{CuW}_{11}O_{39}]^{6-}$ ($X = Si^{IV}$ or Ge^{IV}) for **3**–**6**, respectively. Compare **2** with **3–6**, 1-D linear polymeric chains of them are radically different. The 1-D polymeric chain of **2** is built up from $[\alpha\text{-PCuW}_{11}O_{39}Cl]^{6-}$ polyoxoanions by $[Cu(en)_2]^{2+}$ cations via W–O–Cu–Cl–Cu linkers (Fig. 2c), in contrast, those of **3–6** are formed by $[\alpha\text{-}X\text{CuW}_{11}O_{39}]^{6-}$ ($X = Si^{IV}$ or Ge^{IV}) polyoxoanions via sharing terminal oxygen atoms (Fig. 3c and d). Recently, a 1-D zigzag chain-like silver

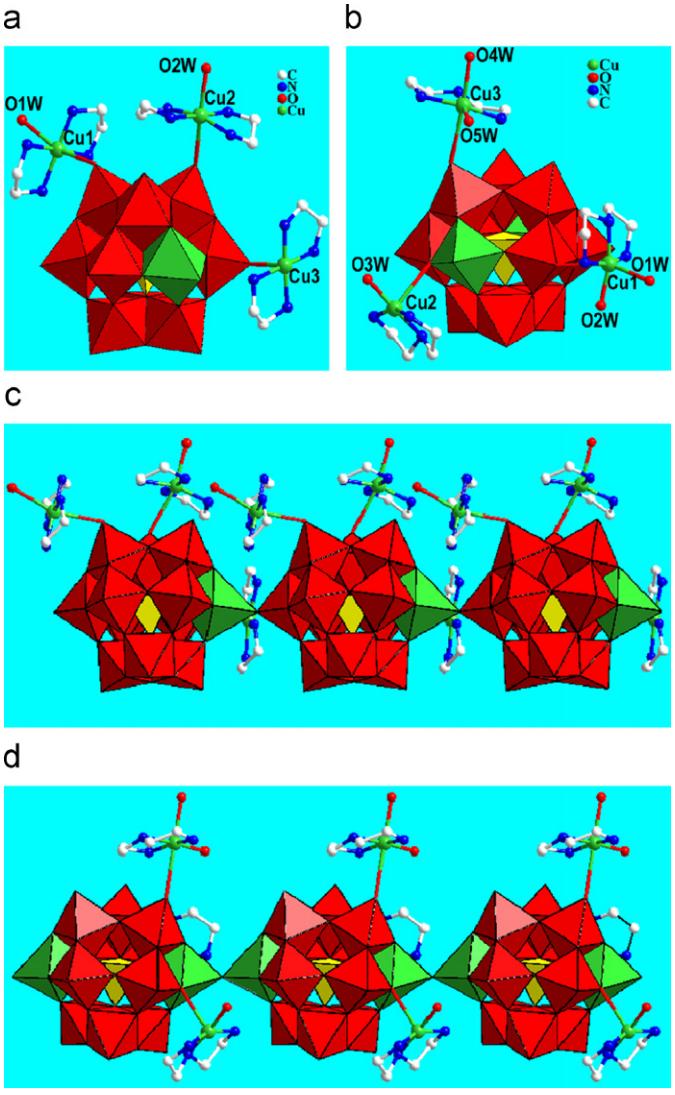

Fig. 3. Combined polyhedral/ball-and-stick representations of the structural unit of **3** (a) and **5** (b) with the selected atomic numbering scheme. In **3**, the Cu4 atom is perfectly located in the defect site of the polyoxoanion $[\alpha\text{-SiCuW}_{11}O_{39}]^{6-}$, while in **5**, the W1 and Cu4 sites are simultaneously occupied by the Cu^{II} and W^{VI} atoms with half occupancy for each in two opposite W_3O_{13} trimers of the polyoxoanion $[\alpha\text{-GeCuW}_{11}O_{39}]^{6-}$. (c) The 1-D polymeric chain in **3** constructed from the monomeric polyoxoanions $[\alpha\text{-SiCuW}_{11}O_{39}]^{6-}$ via the Cu–O–W linkers. (d) The 1-D polymeric chain in **5** constructed from the monomeric polyoxoanions $[\alpha\text{-GeCuW}_{11}O_{39}]^{6-}$ via the Cu/W–O–Cu/W linkers. $\{WO_6\}$: red octahedron; $\{XO_4\}$ (X = Si or Ge): yellow tetrahedron; $\{CuO_6\}$ in the vacant site: green octahedron. The hydrogen atoms attached to the carbon and nitrogen atoms and lattice water molecules are omitted for clarity. For interpretation of the references to colour in this figure legend, the reader is referred to the web version of this article.

tungstophosphate $[\alpha\text{-}PAgW_{11}O_{39}]_n^{6n-}$ was addressed by Nogueira et al. [68] in 2006, in which Ag^{I} cations, exhibiting an unusual eight-coordinate square antiprismatic fashion, bridge a mono-vacant $[\alpha\text{-}PW_{11}O_{39}]^{7-}$ fragment to four bridging μ_2–O atoms of a neighboring mono-vacant α-Keggin fragment (Fig. 4a). On the other hand, several 1-D polymeric chain-like structures and a 1-D double-parallel chain-like arrangement have been reported for lanthanide complexes of mono-vacant α-Keggin polyoxoanions [26–31], five typical 1-D connection motifs are given in Fig. 4b–f. Since the first two 1-D zigzag chain-like lanthanide complexes of mono-vacant α-Keggin anions $(NH_4)_5[Ln(\alpha\text{-}SiW_{11}O_{39})(H_2O)_3]\cdot nH_2O$ ($Ln = Ce^{III}$ or La^{III}) (Fig. 4c) were reported by Pope and co-workers in 2000, to date, this system has been extensively surveyed [26–31]. Several mono-vacant Keggin lanthanide derivatives $[Yb(\alpha\text{-}SiW_{11}O_{39})(H_2O)_2]^{5-}$ [27], $[Ln(\alpha\text{-}GeW_{11}O_{39})(H_2O)_2]^{5-}$ ($Ln = Yb^{III}$ or Y^{III}) [29], $\{Sm(H_2O)_7[Sm(H_2O)_2(DMSO)(\alpha\text{-}SiW_{11}O_{39})]\}^{2-}$ [28] (DMSO = dimethylsulfoxide) and $\{Dy(H_2O)_7[Dy(H_2O)_2(DMSO)(\alpha\text{-}GeW_{11}O_{39})]\}^{2-}$ [28] exhibit the infinite 1-D linear connection motif of Fig. 4b, where each lanthanide ion present in the vacant sites participates in the construction of the 1-D linear chain. This arrangement fashion is intimately related to those of **3–6**. A neodymium complex $[Nd_2(\alpha\text{-}SiW_{11}O_{39})(H_2O)_{11}]^{2-}$ [27] shows the 1-D zigzag connection motif of Fig. 4d, where two kinds of Nd^{III} ions participate in the formation of the 1-D zigzag chain. In $K_3\{[Pr(H_2O)_4(\alpha\text{-}SiW_{11}O_{39})](NaPr_2(H_2O)_{12})[Pr(H_2O)_4(\alpha\text{-}SiW_{11}O_{39})]\}\cdot 13.5H_2O$ [30], the connection motif of Fig. 4e was found, in which the unexpected sodium ions as well as two kinds of praseodymium ions take part in the formation of the 1-D zigzag chain. Interestingly, a novel 1-D double-parallel polymeric chain-like structure was observed in $[Sm_2(\alpha\text{-}GeW_{11}O_{39})(DMSO)_3(H_2O)_6]^{2-}$ (Fig. 4f) [29], in which two kinds of samarium ions, respectively, participate in the connections of intra- and inter-chain architectures. In a word, lanthanide complexes of mono-vacant α-Keggin polyoxoanions have more diverse and complicated architectural fashions than TM complexes of mono-vacant α-Keggin polyoxoanions, mainly because the lanthanide ions have more multiple coordination requirements than transition metals.

The molecular structural unit of **7** contains two discrete planar square $[Cu(dap)_2]^{2+}$ cations [Cu–N: 1.84(2)–2.012(19) Å] and a $\{[Cu(dap)_2]_2[Cu(dap)_2][\alpha\text{-}PCuW_{11}O_{39}]_2\}^{4-}$ dimeric polyoxoanion, which can be described as the condensation of a couple of centrosymmetrically related $\{[Cu(dap)_2][Cu(dap)_2]_{0.5}[\alpha\text{-}PCuW_{11}O_{39}]\}^{2-}$ units by sharing two terminal oxygen atoms through two Cu–O–W bridges (Fig. 5a). However, the two bridges in this case can clearly be determined because the $copper^{II}$ atom is perfectly located in each position, with W3–O11 = 1.774(12) Å and Cu4–O11 = 2.184(13) Å. The pendant six-coordinate $[Cu1(dap)_2]^{2+}$ [Cu–O_t: 2.657(11) Å and Cu–N: 1.988(16)–1.998(13) Å] and five-coordinate $[Cu3(dap)_2]^{2+}$ [Cu–O_b: 2.663(11) Å and Cu–N: 1.982(18)–2.025(15) Å] cations are grafted to the POM through terminal and bridging oxygen atoms, respectively. Interestingly, adjacent $\{[Cu(dap)_2]_2[Cu(dap)_2][\alpha\text{-}PCuW_{11}O_{39}]_2\}^{4-}$ dimeric polyoxoanions are interconnected via $[Cu1(dap)_2]^{2+}$ bridges through W1–O1–Cu1–O1–W1 linkers [W1–O1 = 1.701(12) Å and Cu1–O1 = 2.657(11) Å] generating a novel 1-D infinite polymeric chain along the crystallographic [001] direction (Fig. 5b). In the *ab* plane, 1-D infinite polymeric chains are arranged in parallel with each other viewed down the [100] direction, and discrete $[Cu2(dap)_2]^{2+}$ cations distribute the interspaces formed by polymeric chains, whereas 1-D infinite polymeric chains are packed in the beautiful S-shaped motif viewed down the [010] direction (Fig. 5c).

Notably, the firstly observed dimeric unit $[\alpha\text{-}PCuW_{11}O_{39}]_2^{10-}$ in **7** (Fig. 6a) is obviously distinct from those previously reported dimeric units $[(\alpha\text{-}SiCuW_{11}O_{39})_2(H_2O)]^{12-}$ in $K_8[\{Si_2W_{22}Cu_2O_{78}(H_2O)\}\{Cu_2(ac)_2(phen)_2(H_2O)\}_2]\cdot 40H_2O$ (ac = CH_3COO^-, phen = phenanthroline) [25], $[(\alpha\text{-}PTiW_{11}O_{39})_2(OH)]^{7-}$ in $(Bu_4N)_7[(PTiW_{11}$

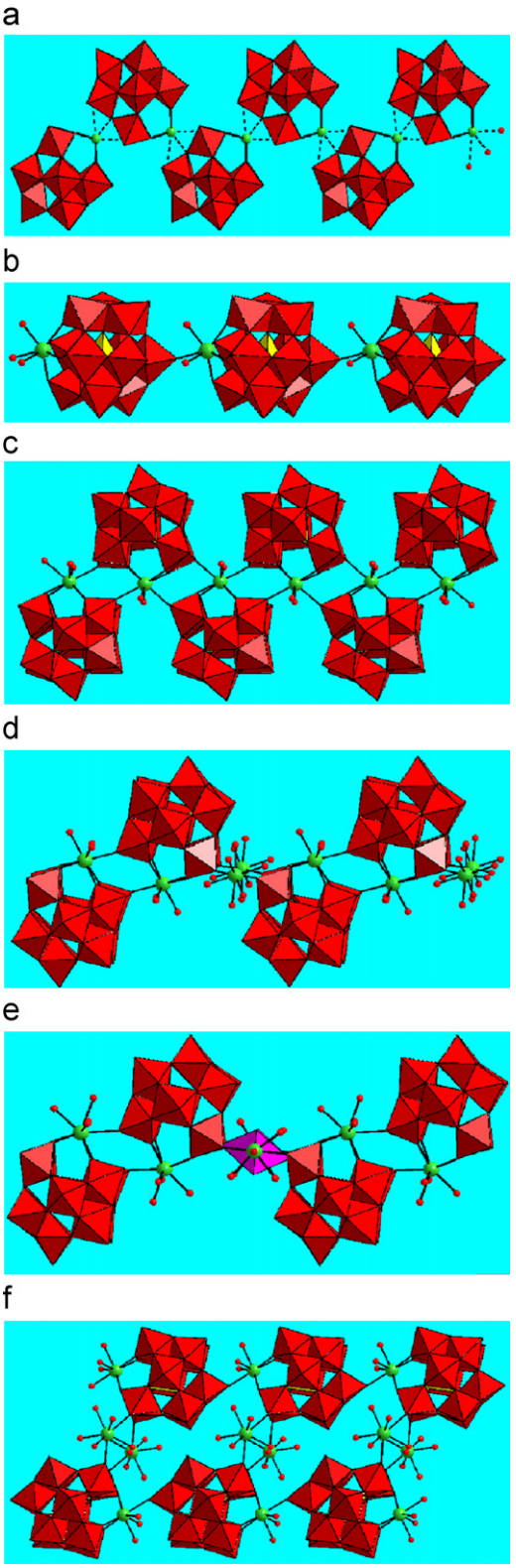

Fig. 4. (a) The 1-D zigzag polymeric chain constructed from the $[\alpha\text{-}PW_{11}O_{39}]^{7-}$ polyoxoanions and the Ag^+ bridges. (b)–(e) The infinite 1-D polymeric chains constructed from the $[\alpha\text{-}XW_{11}O_{39}]^{7/8-}$ polyoxoanions and the Ln^{3+} bridges. (f) The infinite 1-D double-parallel polymeric chain constructed from the $[\alpha\text{-}GeW_{11}O_{39}]^{8-}$ polyanions and the Sm^{3+} bridges. {WO_6}: red octahedron; {XO_4} (X = P, Si or Ge): yellow tetrahedron; Ag^+ and Ln^{3+}: green balls; {NaO_6}: purple octahedron. The hydrogen, carbon and sulfur atoms from DMSO ligands are omitted for clarity. For interpretation of the references to colour in this figure legend, the reader is referred to the web version of this article.

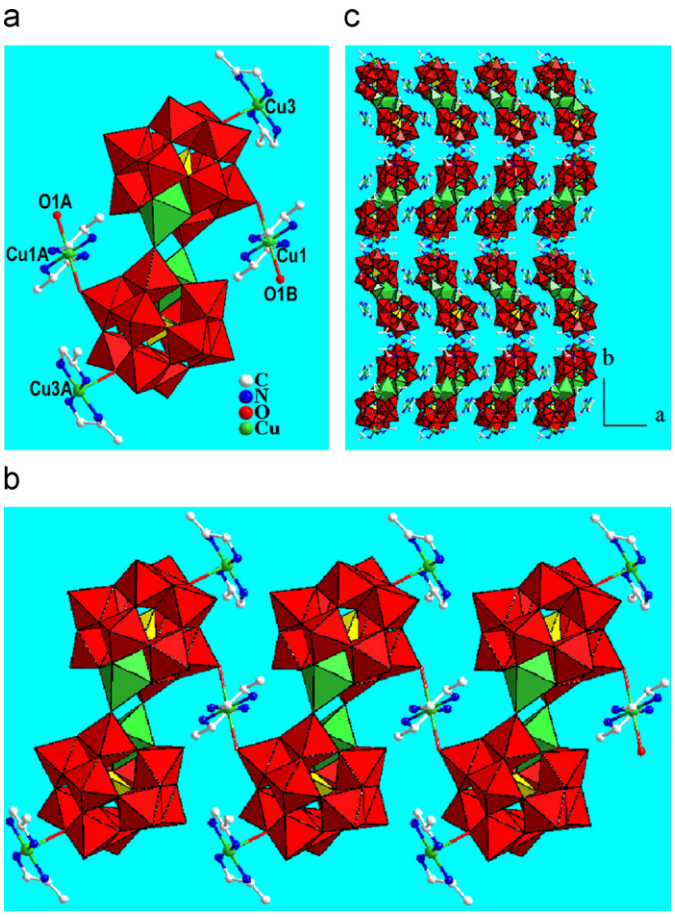

Fig. 5. (a) Combined polyhedral/ball-and-stick representation of the molecular structural unit of **7** with selected atom numbering scheme. {WO_6}: red octahedron; {PO_4}: yellow tetrahedron; {CuO_6} in the vacant site: green octahedron. The atoms with the suffix A and B are generated by the symmetry operation: x, y, $1+z$ for Cu1A and O1A; $1-x$, $-y$, $1-z$ for Cu3A; $1-x$, $-y$, $1-z$ for Cu4A; $1-x$, $-y$, $-z$ for O1B. (b) The 1-D polymeric chain constructed from the dimeric polyoxoanions via the $[Cu1(dap)_2]^{2+}$ bridges through W–O–Cu–O–W linkages in **7**. In (a) and (b), the discrete $[Cu2(dap)_2]^{2+}$ cations and hydrogen atoms attached to carbon and nitrogen atoms are omitted for clarity. (c) The S-shaped arrangement of the polymeric chains, and the discrete $[Cu2(dap)_2]^{2+}$ cations are filled with the interspaces between the polymeric chains. The hydrogen atoms attached to carbon and nitrogen atoms are omitted for clarity. For interpretation of the references to colour in this figure legend, the reader is referred to the web version of this article.

$O_{39})_2(OH)]$ [69] (Fig. 6b), $[Zr(\alpha\text{-}PW_{11}O_{39})_2]^{10-}$ in $(Et_2NH_2)_{10}[Zr(\alpha\text{-}PW_{11}O_{39})_2]\cdot 7H_2O$ [70] and $[Hf(\alpha\text{-}PW_{11}O_{39})_2]^{10-}$ in $(Et_2NH_2)_{10}[Hf(\alpha\text{-}PW_{11}O_{39})_2]\cdot 2H_2O$ [70] (Fig. 6c). Their major discrepancies are summarized as follows: The dimeric unit $[\alpha\text{-}PCuW_{11}O_{39}]_2^{10-}$ in **7** is built by a couple of centrosymmetrically related $[\alpha\text{-}PCuW_{11}O_{39}]^{5-}$ fragments by sharing two terminal oxygen atoms through two Cu–O–W bridges, whereas the dimeric units $[(\alpha\text{-}SiCuW_{11}O_{39})_2(H_2O)]^{12-}$ in $K_8[\{Si_2W_{22}Cu_2O_{78}(H_2O)\}\{Cu_2(ac)_2(phen)_2(H_2O)\}_2]\cdot 40H_2O$ and $[(\alpha\text{-}PTiW_{11}O_{39})_2(OH)]^{7-}$ in $(Bu_4N)_7[(PTiW_{11}O_{39})_2(OH)]$ are composed of a couple of centrosymmetrically related $[\alpha\text{-}SiCuW_{11}O_{39}]^{6-}$ or $[\alpha\text{-}PTiW_{11}O_{39}]^{3-}$ fragments by sharing one water or hydroxy groups through one Cu–O–Cu or Ti–O–Ti bridge, respectively, and the dimeric units $[Zr(\alpha\text{-}PW_{11}O_{39})_2]^{10-}$ in $(Et_2NH_2)_{10}[Zr(\alpha\text{-}PW_{11}O_{39})_2]\cdot 7H_2O$ and $[Hf(\alpha\text{-}PW_{11}O_{39})_2]^{10-}$ in $(Et_2NH_2)_{10}[Hf(\alpha\text{-}PW_{11}O_{39})_2]\cdot 2H_2O$ are constructed by two $[\alpha\text{-}PW_{11}O_{39}]^{7-}$ fragments by sharing an eight-coordinate Zr^{4+} and Hf^{4+} cation. Although dimeric mono-vacant Dawson polyoxoanions $[\{Nd(H_2O)_8\}_2\{Nd(H_2O)_3(\alpha_2\text{-}P_2W_{17}O_{61})\}_2]^{8-}$ [71] and $[\{Ce(H_2O)_4(\alpha_1\text{-}P_2W_{17}O_{61})\}_2]^{14-}$ [72] linked by two rare-earth bridges have also been reported, to the best of our knowledge, compound **7** still represents the first 1-D zigzag chain architecture constructed from dimeric monocopper^{II}-substituted Keggin polyoxoanions and copper^{II}–organoamine cations with the type of $-A-B-A-B-$ ($A=[\alpha\text{-}PCuW_{11}O_{39}]_2^{10-}$, $B=[Cu(en)_2]^{2+}$.

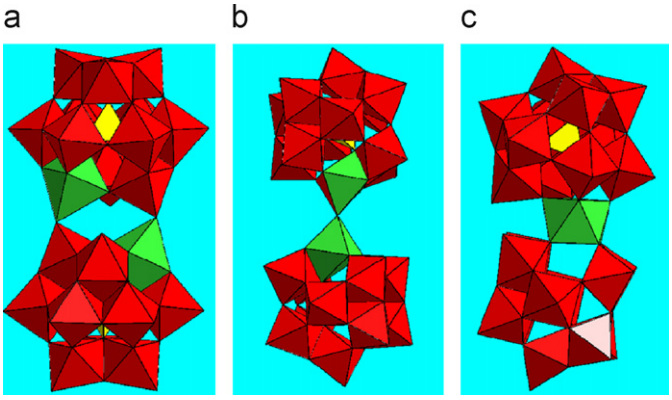

Fig. 6. Polyhedral representations of the dimeric units: (a) $[\alpha\text{-}PCuW_{11}O_{39}]_2^{10-}$ in **7**; (b) $[(\alpha\text{-}SiCuW_{11}O_{39})_2(H_2O)]^{12-}$ and $[(\alpha\text{-}PTiW_{11}O_{39})_2(OH)]^{7-}$ in $K_8[\{Si_2W_{22}Cu_2O_{78}(H_2O)\}\{Cu_2(ac)_2(phen)_2(H_2O)\}_2]\cdot 40H_2O$ and $(Bu_4N)_7[(PTiW_{11}O_{39})_2(OH)]$; (c) $[Zr(\alpha\text{-}PW_{11}O_{39})_2]^{10-}$ and $[Hf(\alpha\text{-}PW_{11}O_{39})_2]^{10-}$ in $(Et_2NH_2)_{10}[Zr(\alpha\text{-}PW_{11}O_{39})_2]\cdot 7H_2O$ and $(Et_2NH_2)_{10}[Hf(\alpha\text{-}PW_{11}O_{39})_2]\cdot 2H_2O$, respectively. {$WO_6$}: red octahedron; {$XO_4$}: yellow tetrahedron; {$CuO_6$}, {$TiO_6$}, {$ZrO_8$} or {$HfO_8$} in the vacant site: green octahedron or square antiprism. For interpretation of the references to colour in this figure legend, the reader is referred to the web version of this article.

It should be mentioned that the design and assembly of metal-involved supramolecular architectures are currently of great interest in the field of supramelocular chemistry and crystal engineering because they can provide novel topology and functional materials [73,74]. Moreover, Keggin-based supramolecular architectures are regarded as one of the most promising materials potentially applied in the field of chemistry, biology and material sciences [75–77]. From the viewpoint of supramelocular chemistry, supramolecular architectures are also present in compounds **1–7** regarding of hydrogen-bonding interactions between nitrogen atoms of organoamine ligands and surface oxygen atoms of polyoxoanions, water molecules or chlorine ions. Specifically, organoamine ligands on copper complex cations act as the proton donors, surface oxygen atoms of monocopper^{II}-substituted Keggin polyoxoanions and water molecules work as the proton acceptors, and then donors and acceptors are hydrogen-bonded together generating the infinitely 3-D extended supramolecular networks. The N–H···O distances are in the range of 2.909(13)–3.445(13) Å for **1**, 2.88(3)–3.430(18) Å for **2**, 2.85(2)–3.38(2) Å for **3**, 2.90(3)–3.29(3) Å for **4**, 2.90(3)–3.40(3) Å for **5**, 2.92(3)–3.43(3) Å for **6** and 2.93(2)–3.34(2) Å for **7**, respectively (Table 2). In the case of **1** and **2**, chlorine ions also function as proton acceptors in addition to monocopper^{II}-substituted Keggin polyoxoanions and water molecules as proton acceptors. The N–H···Cl distances are 3.291(13) Å for **1** and 3.231(11) Å for **2**, respectively. The N–H···X (X = Cl, Br, I) halogen-bonding interactions have been found in many supramolecular compounds [78,79]. Moreover, halogen-bonding interactions have been identified as key components in synthons employed in organic crystal engineering because the strength of a halogen bond is comparable to that of many hydrogen bonds [80]. In short, the formation of these supramolecular interactions may be somewhat responsible for enhancing the chemical stability of **1–7**.

3.3. IR spectroscopy

The FT-IR spectra for **1–7** display the strong characteristic vibration bands in the 1200–400 cm^{-1} region (Fig. 7) [24,81], very

Table 2
The hydrogen bonding interactions for **1–7**

Compounds	Distances of N–H···Cl (Å)	Angles of N–H···Cl (deg)	Distances of N–H···O (Å)	Angles of N–H···O (deg)
1	3.291(13)	164.0	2.909(13)–3.445(13)	116.7–171.4
2	3.231(11)	170.1	2.88(3)–3.430(18)	118.1–175.7
3	–	–	2.85(2)–3.38(2)	113.7–174.6
4	–	–	2.90(3)–3.29(3)	110.7–176.1
5	–	–	2.90(3)–3.40(3)	114.3–177.2
6	–	–	2.92(3)–3.43(3)	112.9–173.8
7	–	–	2.93(2)–3.34(2)	122.3–173.0

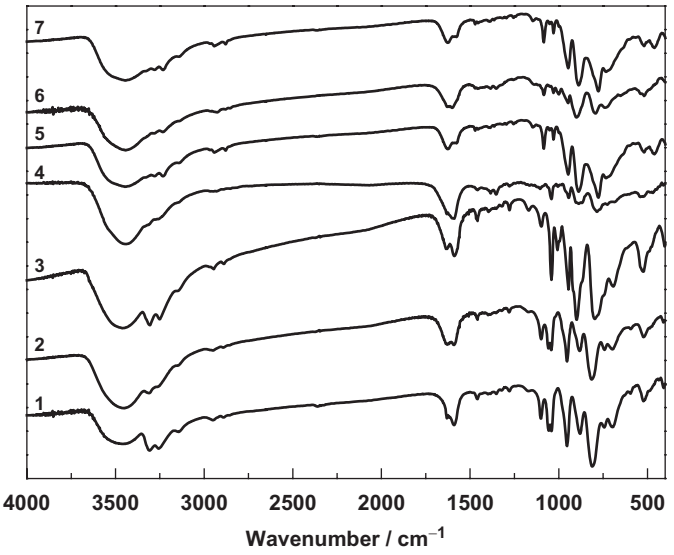

Fig. 7. The FT-IR spectra of **1–7** collected as the KBr pellets in the range of 4000–400 cm^{-1}.

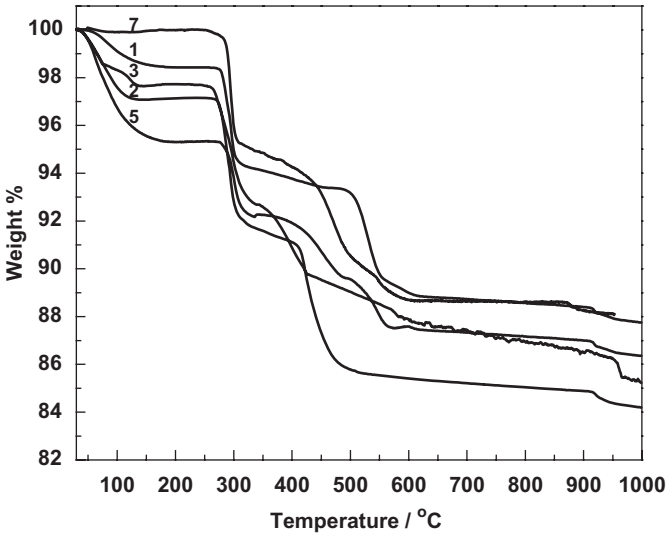

Fig. 8. The TGA curves of **1**, **2**, **3**, **5** and **7** on crystalline samples in an air atmosphere in the range of 30–1000 °C.

similar to those of parent mono-vacant polyanions $[\alpha\text{-}XW_{11}O_{39}]^{7/8-}$ ($X = P^{V}$, Si^{IV} or Ge^{IV}) due to the fact that the polyoxoanions exhibit the same C_s symmetry. The W–O stretching vibration bands resulting from the Keggin-type structure, namely, $\nu(W\text{–}O_t)$, $\nu(W\text{–}O_b)$ and $\nu(W\text{–}O_c)$ appear at 951, 879 and 810–698 cm^{-1} for **1**; 951, 883 and 814–698 cm^{-1} for **2**; 943, 899 and 790–677 cm^{-1} for **3**; 943, 887 and 786–681 cm^{-1} for **4**; 943, 887 and 774–730 cm^{-1} for **5**; 947, 899 and 794–734 cm^{-1} for **6**; and 951, 874 and 810–694 cm^{-1} for **7**, respectively. In general, these characteristic bands can be easily assigned by comparing with the corresponding bands of mono-vacant or plenary Keggin clusters. The $\nu(X\text{–}O_a)$ mode, observed as a single signal in the region 1080–980 cm^{-1} for plenary Keggin clusters $[XW_{12}O_{40}]^{3/4-}$ [24], splits into two bands in the spectra of monocopper^{II}-substituted derivatives **1–7**, which appear as very weak shoulders of the $\nu(W\text{–}O_t)$ band for the Ge^{IV}-containing POMs. These values correlate very well to the $X\text{–}O_a$ bond distances, that is, the higher $\nu(X\text{–}O_a)$ values correspond to the shorter $X\text{–}O_a$ bond distances. The $X\text{–}O_a$ stretching band is split into two bands in the spectra mainly owing to a consequence of the distortion of the XO_4 group encapsulated in Keggin polyoxoanions. Indeed, it has been observed that the P–O asymmetric stretching vibration splits into two bands in the mono-TM-substituted $[PW_{11}MO_{39}]^{5-}$ complexes and that the splitting value depends on the strength of the $M\text{–}O(PO_3)$ bond [82,83]. The splitting is larger for $M = Cu^{II}$ with observed frequencies equal to 1065 and 1105 cm^{-1} for the potassium salt of $[PW_{11}CuO_{39}]^{5-}$ [83]. Furthermore, the $\nu(W\text{–}O_c)$ stretching vibration bands for **1–7** also splits into two or three bands as a result of the lower symmetry of monocopper^{II}-substituted polyoxoanions in **1–7** than that of plenary Keggin clusters. In the 750–650 cm^{-1} region, the vibration bands are involved in $\nu(Cu\text{–}O)$ modes mixed with $\nu(W\text{–}O_c)$ bands. These vibration bands are red-shifted as the heteroatom changes from P^{V}, Si^{IV} to Ge^{IV}. These results are in good consistence with the previous reports [24]. Additionally, a close examination of IR spectra for **1–7** reveals that the red-shifts of $\nu(W\text{–}O_t)$ vibration frequencies are observed in comparison with those of corresponding mono-vacant polyoxoanions $[\alpha\text{-}XW_{11}O_{39}]^{7/8-}$, which may stem from stronger interactions between terminal oxygen atoms and copper–organoamine cations. The stretching bands of the –OH, $–NH_2$ and $–CH_2$ groups are observed at 3420–3460, 3120–3350 and 2950–3000 cm^{-1}, respectively. The bending vibration bands of $–NH_2$ and $–CH_2$ groups appear at 1590–1630 and 1455–1465 cm^{-1}, respectively. The occurrence of these signals is indicative of the presence of organoamines, being in good agreement with single-crystal structural analyses.

3.4. Thermogravimatric analysis (TGA)

The thermal stability of **1**, **2**, **3**, **5** and **7** were investigated on crystalline samples under an air atmosphere from 30 to 1000 °C (Fig. 8). The TGA curve indicates the weight loss of **1** can be divided into three steps. The first weight loss is 1.55% (calc. 1.59%) from 30 to 270 °C, involving the release of three lattice water molecules. The second weight loss is 5.15% (calc. 6.31%) from 270 to 490 °C, approximately assigned to the removal of two coordinated water molecules and the decomposition of three en ligands. The third weight loss is 5.51% (calc. 5.25%) between 490 and 1000 °C, attributable to the decomposition of three en ligands.

The TGA curve of **2** is very similar to that of **1,** also showing three weight-loss steps. One weight loss (2.80%) between 30 and 268 °C corresponds to the loss of six lattice water molecules (calc. 3.13%). Another weight loss of 6.00% between 268 and 396 °C is attributed to the removal of one coordinated water molecule and the decomposition of three en ligands (calc. 5.74%). After 396 °C, a gradual weight loss of 6.19% until 1000 °C is observed and approximately assigned to the decomposition of three en ligands (calc. 5.22%).

The TGA curve indicates that the weight loss of **3** can be divided into three steps. The first weight loss is 2.93% from 30 to 254 °C, corresponding to the release of five lattice water molecules (calc. 2.65%). The combined weight loss of the second and third steps is 12.30% between 254 and 1000 °C, assigned to the removal of two coordinated water molecules and six en ligands (calc. 11.62%).

The TGA curve shows that compound **5** decomposes via three steps of weigh loss. The first one is a dehydration process below 275 °C [found (calc.) for five lattice water molecules and four coordinated water molecules: 4.67% (4.68%)], followed by the release of one coordinated water molecule and one deta ligand [3.44% (3.53%)] between 275 and 402 °C. After then, compound **5** undergoes the loss of two deta ligands [5.49% (calc. 6.02%)] from 402 to 1000 °C.

In the case of compound **7**, it is anhydrous and thermally stable up to relatively high temperature (260 °C), after which it undergoes a two-step loss weight processes from 260 to 1000 °C. The weight loss of 4.79% during the first step from 260 to 332 °C involves the loss of four dap ligands on the discrete $[Cu2(dap)_2]^{2+}$ cations (calc. 4.52%). On further heating, the second weight loss is 7.11% between 332 and 1000 °C, corresponding to the removal of six dap ligands on the coordinated $[Cu1(dap)_2]^{2+}$ and $[Cu3(dap)_2]^{2+}$ cations (calc. 6.78%).

3.5. Electronic spin resonance (ESR) spectra of 7

X-band powder ESR spectra of **7** recorded at room temperature and 77 K are shown in Fig. 9. The room temperature X-band spectrum displays a broad anisotropic resonance at ca. 3200 G with $g_{\|} = 2.155$, $A_{\|} = 138.7$ G and $g_{\perp} = 2.100$. When the systems are cooled, the resolution improves considerably, as a result of the signal narrowing induced apparently by the increasing spin-lattice relaxation time [23,25]. At 77 K, the intense central line gives rise to an evident axial signal with $g_{\|} = 2.149$, $A_{\|} = 145.5$ G and $g_{\perp} = 2.105$ that clearly shows four copper hyperfine lines originated by a spin doublet $S = 1/2$ interacting with a single $I = 3/2$ nucleus in the low-field region [23]. These signals are characteristic of the isolated Cu^{II} chromophores with an axial g tensor and prove that Cu^{II} ions reside in the square pyramidal or octahedral stereochemistry [84]. The spin Hamiltonian parameters of Cu^{II} ions are very sensitive to the surrounding ligands and to their site symmetry. For instance, Cu^{II} ions with tetrahedral symmetry have spin Hamiltonian parameters in the range of $g_{\|} = 2.516$ and $A_{\|} = 0.007\,cm^{-1}$, while with square planar symmetry the parameters are in the range of $g_{\|} = 2.245$ and $A_{\|} = 0.017\,cm^{-1}$ [84]. Spin Hamiltonian parameters for Cu^{II} ions with distorted octahedral and square pyramidal symmetry are related to these values [85,86]. Moreover, if nitrogen atoms are coordinated to Cu^{II} ions with a given symmetry, the $A_{\|}$ value increases and the $g_{\|}$ value decreases as compared to the cupric ions coordinated by oxygen atoms with the same symmetry. For example, the parameters $g_{\|} = 2.24$ and $A_{\|} = 0.017\,cm^{-1}$ for nitrogen atoms coordinated to Cu^{II} ions indicate an octahedral complex instead of a square planar one [87]. In **7**, the coordination of dap ligands to Cu^{II} ions also leads to decreasing the $g_{\|}$ value.

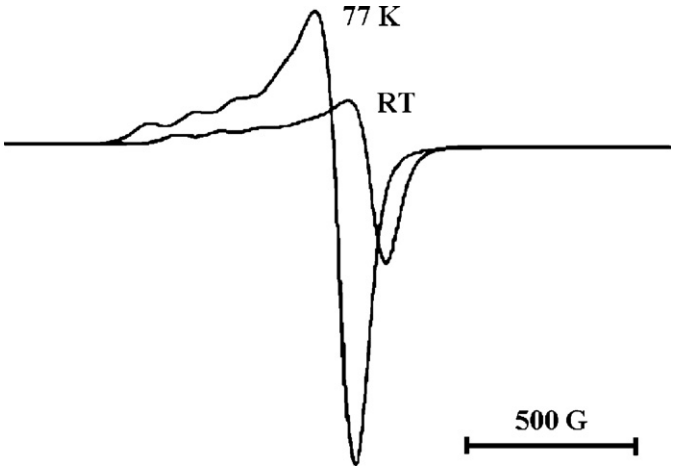

Fig. 9. X-band powder ESR spectra of **7** measured at room temperature and 77 K.

4. Conclusion

Seven inorganic–organic composite POTs have been harvested by combination of in-situ generated monocopper^{II}-substituted Keggin polyoxoanions and copper^{II}–organoamine complexes based on di-/tri-/hexa-vacant polyoxoanion precursors, $CuCl_2 \cdot 2H_2O$ and organoamines under hydrothermal conditions and structurally characterized by the elemental analysis, IR spectroscopy, TGA and single-crystal X-ray crystallography. Their common structural features are that all are composed of monocopper^{II}-substituted α-Keggin polyoxoanions as fundamental building units, on which copper–organoamine complexes are supported as pendants. As the result of the Jahn–Teller distortion, the axially elongated octahedral geometry of Cu^{II} ions plays an important role in the structural constructions. These results reveal the extreme structural versatility in POM chemistry and let us expect that a large class of the inorganic–organic composite polymeric POTs could be obtained in this way by varying the nature of TM cations and organic ligands. The successful syntheses of **1**–**7** provide some experimental evidences that di-/tri-/hexa-vacant polyoxoanions can be transformed into monovacant Keggin polyoxoanions under hydrothermal conditions.

Acknowledgments

The authors are thankful for the financial supports from the National Natural Science Fund for Distinguished Young Scholars of China (no. 20725101), the 973 Program (no. 2006CB932904), the NSF of Fujian Province (no. E0510030) and the Knowledge Innovation Program of the Chinese Academy of Sciences (no. KJCX2.YW.H01).

References

[1] J. Berzelius, Pogg. Ann. 6 (1826) 369.
[2] J.F. Keggin, Proc. R. Soc. London Ser. A 144 (1934) 75.
[3] E.B. Wang, C.W. Hu, L. Xu, Introduction of Polyacid Chemistry, Chemical Industry Press, Beijing, 1998.
[4] A. Proust, Actual. Chim. (2000) 55.
[5] S. Reinoso, P. Vitoria, L.S. Felices, A. Montero, L. Lezama, J.M. Gutiérrez-Zorrilla, Inorg. Chem. 46 (2007) 1237.
[6] M.T. Pope, Heteropoly and Isopoly Oxometalates, Springer, Berlin, 1983.
[7] J.J. Borrás-Almenar, E. Coronado, A. Müller, M.T. Pope, Polyoxometalate Molecular Science, Kluwer Academic Publishers, Dordrecht, The Netherlands, 2003.
[8] C.L. Hill, Chem. Rev. 98 (1998) 1.
[9] T. Okuhara, N. Mizuno, M. Misono, Adv. Catal. 41 (1996) 113.
[10] G. Chottard, C.L. Hill, M.S. Weeks, R.F. Schinazi, J. Med. Chem. 33 (1990) 2767.
[11] U. Kortz, F. Hussain, M. Reicke, Angew. Chem. Int. Ed. 44 (2005) 2.
[12] T. Yamase, P.V. Prokop, Angew. Chem. Int. Ed. 41 (2002) 466.
[13] Y. Xu, J.Q. Xu, K.L. Zhang, Y. Zhang, X.Z. You, Chem. Commun. (2000) 153.

[14] J.Y. Niu, M.L. Wei, J.P. Wang, D.B. Dang, Eur. J. Inorg. Chem. (2004) 160.
[15] A. Dolbecq, P. Mialane, L. Lisnard, J. Marrot, F. Sécheresse, Chem. Eur. J. 9 (2003) 2914.
[16] M. Yaun, Y. Li, E. Wang, C. Tian, L. Wang, N. Hu, H. Jia, Inorg. Chem. 42 (2003) 3670.
[17] H. Zhang, L.Y. Duan, Y. Lan, E.B. Wang, C.W. Hu, Inorg. Chem. 42 (2003) 8053.
[18] J.R. Galán-Mascarós, C. Giménez-Saiz, S. Triki, C.J. Gómez-Garcia, E. Coronado, L. Ouahab, Angew. Chem. Int. Ed. Engl. 34 (1995) 1460.
[19] H.T. Evans, T.J.R. Weakley, G.B. Jameson, J. Chem. Soc. Dalton Trans. (1996) 2537.
[20] B.B. Yan, Y. Xu, X.H. Bu, N.K. Goh, L.S. Chia, G.D. Stucky, J. Chem. Soc. Dalton Trans. (2001) 2009.
[21] L. Lisnard, A. Dolbecq, P. Mialane, J. Marrot, F. Sécheresse, Inorg. Chim. Acta 357 (2004) 845.
[22] Y. Lu, Y. Xu, E.B. Wang, J. Lü, C.W. Hu, L. Xu, Cryst. Growth Des. 5 (2005) 257.
[23] S. Reinoso, P. Vitoria, J.M. Gutiérrez-Zorrilla, L. Lezama, L.S. Felices, J.I. Beitia, Inorg. Chem. 44 (2005) 9731.
[24] L.S. Felices, P. Vitoria, J.M. Gutiérrez-Zorrilla, L. Lezama, S. Reinoso, Inorg. Chem. 45 (2006) 7748.
[25] S. Reinoso, P. Vitoria, L.S. Felices, L. Lezama, J.M. Gutiérrez-Zorrilla, Inorg. Chem. 45 (2006) 108.
[26] M. Sadakane, M.H. Dickman, M.T. Pope, Angew. Chem. Int. Ed. 39 (2000) 2914.
[27] P. Mialane, L. Lisnard, A. Mallard, J. Marrot, E. Antic-Fidancev, P. Aschehoug, D. Vivien, F. Sécheresse, Inorg. Chem. 42 (2003) 2102.
[28] J.P. Wang, J.W. Zhao, X.Y. Duan, J.Y. Niu, Cryst. Growth Des. 6 (2006) 507.
[29] J.P. Wang, X.Y. Duan, X.D. Du, J.Y. Niu, Cryst. Growth Des. 6 (2006) 2266.
[30] J.Y. Niu, J.W. Zhao, J.P. Wang, Inorg. Chem. Commun. 7 (2004) 876.
[31] F.L.S. Sousa, F.A. Almeida Paz, C.M.C.E. Granadeiro, A.M.V. Cavaleiro, J. Rocha, J.K. Klinowski, H.I.S. Nogueira, Inorg. Chem. Commun. 8 (2005) 924.
[32] S.-T. Zheng, D.-Q. Yuan, J. Zhang, G.-Y. Yang, Inorg. Chem. 46 (2007) 4569.
[33] J.-W. Zhao, H.-P. Jia, J. Zhang, S.-T. Zheng, G.-Y. Yang, Chem. Eur. J. 13 (2007) 10030.
[34] J.-W. Zhao, J. Zhang, S.-T. Zheng, G.-Y. Yang, Chem. Commun. (2008) 570.
[35] P.J. Domaille, Inorg. Synth. 27 (1990) 100.
[36] R. Contant, Inorg. Synth. 27 (1990) 108.
[37] A. Tézé, G. Hervé, Inorg. Synth. 27 (1990) 88.
[38] L.H. Bi, U. Kortz, S. Nellutla, A.C. Stowe, J. van Tol, N.S. Dalal, B. Keita, L. Nadjo, Inorg. Chem. 44 (2005) 896.
[39] G.M. Sheldrick, SHELXL-97, Program for Crystal Structure Refinement, University of Göttingen, Göttingen, Germany, 1997.
[40] S. Reinoso, P. Vitoria, L.S. Felices, L. Lezama, J.M. Gutiérrez-Zorrilla, Chem. Eur. J. 11 (2005) 1538.
[41] C. Baerlocher, W.M. Meier, D.H. Olson, Atlas of Zeolite Framework Types, Elsevier, Amsterdam, 2001.
[42] S.T. Zheng, J. Zhang, G.Y. Yang, Inorg. Chem. 44 (2005) 2426.
[43] S.T. Zheng, D.Q. Yuan, H.P. Jia, J. Zhang, G.Y. Yang, Chem. Commun. (2007) 1858.
[44] C.M. Wang, S.T. Yang, G.Y. Yang, Inorg. Chem. 46 (2007) 616.
[45] G. Hervé, A. Tézé, Inorg. Chem. 16 (1977) 2115.
[46] $(H_2en)_2[Cu_8(en)_4(H_2O)_2(B\text{-}\alpha\text{-}SiW_9O_{34})_2]\cdot 8H_2O$: monoclinic, $P2_1/n$, $a = 13.2929(17)$ Å, $b = 21.195(4)$ Å, $c = 15.591(2)$ Å, $\beta = 91.674(7)^\circ$, $V = 4390.6(11)$ Å^3.
[47] $H_4[Cu_8(dap)_4(H_2O)_2(B\text{-}\alpha\text{-}GeW_9O_{34})_2]\cdot 13H_2O$: monoclinic, $P2_1/c$, $a = 13.24380(10)$ Å, $b = 16.5562(2)$ Å, $c = 23.60870(10)$ Å, $\beta = 98.6960(10)^\circ$, $V = 5117.10(8)$ Å^3.
[48] N. Haraguchi, Y. Okaue, T. Isobe, Y. Matssuda, Inorg. Chem. 33 (1994) 1015.
[49] $(H_2en)_{0.5}H[Cu(en)_2(H_2O)]_2\{[Cu(en)_2](\alpha_1\text{-}P_2CuW_{17}O_{61})\}\cdot 8H_2O$: triclinic, $P\text{–}1$, $a = 11.7626(17)$ Å, $b = 13.246(2)$ Å, $c = 29.350(5)$ Å, $\alpha = 87.355(5)^\circ$, $\beta = 79.583(5)^\circ$, $\gamma = 66.993(3)^\circ$, $V = 4138.3(11)$ Å^3.
[50] U. Kortz, S. Nellutla, A.C. Stowe, N.S. Dalal, U. Rauwald, W. Danquah, D. Ravot, Inorg. Chem. 43 (2004) 2308.
[51] W.H. Knoth, P.J. Domaille, R.L. Harlow, Inorg. Chem. 25 (1986) 1577.
[52] C.R. Mayer, R. Thouvenot, J. Chem. Soc. Dalton Trans. (1998) 7.
[53] U. Kortz, I.M. Mbomekalle, B. Keita, L. Nadjo, P. Berthet, Inorg. Chem. 41 (2002) 6412.
[54] T.J.R. Weakley, H.T. Evans Jr., J.S. Showell, G.F. Tourné, C.M. Tourné, J. Chem. Soc. Chem. Commun. (1973) 139.
[55] A. Mazeaud, N. Ammari, F. Robert, R. Thouvenot, Angew. Chem. Int. Ed. Engl. 35 (1996) 1961.
[56] N. Ammari, G. Hervé, R. Thouvenot, New J. Chem. 15 (1991) 607.
[57] J.Y. Niu, M.X. Li, J.P. Wang, J. Organometal. Chem. 675 (2003) 84.
[58] U. Kortz, S. Isber, M.H. Dickman, D. Ravot, Inorg. Chem. 39 (2000) 2915.
[59] B.S. Bassil, U. Kortz, A.S. Tigan, J.M. Clemente-Juan, B. Keita, P. de Oliveira, L. Nadjo, Inorg. Chem. 44 (2005) 9360.
[60] K. Wassermann, H.J. Lunk, R. Palm, J. Fuchs, N. Steinfeldt, R. Stösser, M.T. Pope, Inorg. Chem. 35 (1996) 3273.
[61] X. Zhang, C.J. O'Connor, G.B. Jameson, M.T. Pope, Inorg. Chem. 35 (1996) 30.
[62] F. Xin, M.T. Pope, Inorg. Chem. 35 (1996) 5693.
[63] J. Liu, F. Ortéga, P. Sethuraman, D.E. Katsoulis, C.E. Costello, M.T. Pope, J. Chem. Soc. Dalton Trans. (1992) 1901.
[64] U. Kortz, Y.P. Jeannin, A. Tézé, G. Hervé, S. Isber, Inorg. Chem. 38 (1999) 3670.
[65] M. Zimmermann, N. Belai, R.J. Butcher, M.T. Pope, E.V. Chubarova, M.H. Dickman, U. Kortz, Inorg. Chem. 46 (2007) 1737.
[66] X.M. Chen, J.W. Cai, Single-Crystal Structural Analysis Principles and Practices, Higher Education Press, Beijing, 2003.
[67] B.S. Bassil, S. Nellutla, U. Kortz, A.C. Stowe, J. van Tol, N.S. Dalal, B. Keita, L. Nadjo, Inorg. Chem. 44 (2005) 2659.
[68] H.I.S. Nogueira, F.A. Almeida Paz, P.A.F. Teixeira, J. Klinowski, Chem. Commun. (2006) 2953.
[69] O.A. Kholdeeva, G.M. Maksimov, R.I. Maksimovskaya, L.A. Kovaleva, M.A. Fedotov, V.A. Grigoriev, C.L. Hill, Inorg. Chem. 39 (2000) 3828.
[70] C.N. Kato, A. Shinohara, K. Hayashi, K. Nomiya, Inorg. Chem. 45 (2006) 8108.
[71] Y. Lu, Y. Xu, Y.G. Li, E.B. Wang, X.X. Xu, Y. Ma, Inorg. Chem. 45 (2006) 2055.
[72] M. Sadakane, M.H. Dickman, M.T. Pope, Inorg. Chem. 40 (2001) 2715.
[73] O.M. Yaghi, M. O'Keeffe, N.W. Ockwig, H.K. Chae, M. Eddaoudi, J. Kim, Nature 423 (2003) 705.
[74] B. Moulton, M.J. Zaworotko, Chem. Rev. 101 (2001) 1629.
[75] E. Coronado, C.J. Gómez-García, Chem. Rev. 98 (1998) 273.
[76] N. Mizuno, M. Misono, Chem. Rev. 98 (1998) 199.
[77] P.Q. Zheng, Y.P. Ren, L.S. Long, R.B. Huang, L.S. Zheng, Inorg. Chem. 44 (2005) 1190.
[78] V.R. Pedireddi, D. Shekhar Reddy, G. Satish Goud, D.C. Craig, A. David Rae, G.R. Desiraju, J. Chem. Soc. Perkin Trans. 2 (11) (1994) 2353.
[79] R.B. Walsh, C.W. Padgett, P. Metrangolo, G. Resnati, T.W. Hanks, W.T. Pennington, Cryst. Growth Des. 1 (2001) 165.
[80] C.B. Aakeröy, N. Schultheiss, J. Desper, C. Moore, Cryst. Eng. Commun. 9 (2007) 421.
[81] J.A.F. Gamelas, A.M.V. Cavaleiro, C. Freire, B. De Castro, J. Coord. Chem. 54 (2001) 35.
[82] F. Zonnevijlle, C.M. Tourné, G.F. Tourné, Inorg. Chem. 21 (1982) 2742.
[83] L. Lisnard, A. Dolbecq, P. Mialane, J. Marrot, E. Codjovi, F. Sécheresse, Dalton Trans. (2005) 3913.
[84] A. Murali, Z.X. Chang, K.T. Ranjit, R.M. Krishna, V. Kurshev, L. Kevan, J. Phys. Chem. B 106 (2002) 6913.
[85] H. Tominaga, Y. Ono, T. Keii, J. Catal. 40 (1975) 197.
[86] B.J. Hathaway, D.E. Billing, Coord. Chem. Rev. 5 (1970) 143.
[87] B.J. Hathaway, A.A.G. Tomlinson, Coord. Chem. Rev. 5 (1970) 1.